

OH Maser Observations of Planetary Nebulae Precursors

R. M. Deacon ¹

School of Physics A29, University of Sydney, NSW Australia 2006

`rdeacon@physics.usyd.edu.au`

J. M. Chapman

*CSIRO Australia Telescope National Facility
PO Box 76, Epping, NSW 1710, Australia*

and

A. J. Green

School of Physics, University of Sydney, NSW 2006, Australia

ABSTRACT

We present OH maser observations at 1612, 1665, 1667, and 1720 MHz for 86 post-asymptotic giant branch (post-AGB) stars selected from a survey of 1612 MHz maser sources in the Galactic Plane. The observations were taken with the Parkes Telescope and the Australia Telescope Compact Array between 2002 September and 2003 August. Post-AGB stars are the precursors to planetary nebulae, the diverse morphological range of which is unexplained. The maser observations were taken to investigate the onset and incidence of wind asymmetries during the post-AGB phase. We re-detected all 86 sources at 1612 MHz while 27 sources were detected at 1665 and 45 at 1667 MHz. One source was re-detected at 1720 MHz. We present a classification scheme for the maser profiles and show that 25% of sources in our sample are likely to have asymmetric or bipolar outflows. From a comparison of the maser and far-infrared properties we find that there is a likely trend in the shape of the maser profiles with some sources evolving from double-peaked to irregular to fully bipolar profiles. A subset of higher-mass sources stand out as having almost no mainline emission and mostly double-peaked profiles. At least 25% of sources in the sample are variable at one or more of the frequencies observed. We also confirm a previously-noted 1667 MHz overshoot phenomenon.

¹Affiliated with the Australia Telescope National Facility, CSIRO

Subject headings: masers—stars: AGB and post-AGB—stars: circumstellar matter—stars: evolution—stars: mass loss—radio lines: stars

1. Introduction

Planetary nebulae (PN) are the remnants of low-to-middle mass stars. When stars, like our own sun, run out of core-burning hydrogen, they go through a sequence of structural changes. The outer layers greatly expand while the stellar cores decrease in size and become hotter. Of particular interest in the asymptotic giant branch (AGB) stage is that most stars shed a large fraction of their mass through slow, dense stellar winds. Such winds transfer more than half of a star’s original mass back into the interstellar medium. After most of the outer layers of gas have been shed, it is thought that stars change from losing mass in slow dense winds to losing mass in much hotter, faster winds (Kwok, Purton & Fitzgerald 1978). During this post-AGB stage, the hot winds sweep up the remaining material surrounding the stars and the swept-up shells become visible as PN as the central stars become hot enough to ionise the shells (Kwok et al. 1978).

The ionised shells of PN exhibit many different forms. While some appear circular, more than half have elliptical or bipolar shapes; in some cases with complex, filamentary structures (Manchado et al. 2000). Hubble Space Telescope (HST) observations indicate that approximately 50% of proto-planetary nebulae (the newly-optically visible precursors to PN) also show similar structures (Ueta, Meixner & Bobrowsky 2000; Su, Hrivnak & Kwok 2001). The causes for this proliferation of geometries are not yet known and several different theories are being debated. One possible explanation is that magnetic fields from the stars may constrain or collimate the stellar winds (e.g. García-Segura et al. 1999). Hydrodynamical models show that a bipolar structure may form if the slow AGB wind possesses a weak asymmetry that is amplified during the post-AGB phase by a fast-wind, slow-wind interaction (e.g. Frank & Mellema 1994). In this case, strong bipolar structures are not expected to be present in the early post-AGB phase as the stars are too cool ($< 15\,000$ K) for the onset of a fast wind. However, Sahai & Trauger (1998) have proposed that fast jets operating in the early post-AGB stage may be the dominant shaping mechanism. The origin of these jets is unclear but the influence of companion stars or planets is the most plausible reason. Bipolarity may also arise through other mechanisms linked to the presence of companion stars or planets (Wood 2000; Soker 2001).

OH maser observations provide a means of studying the cooler molecular emission from the outer circumstellar envelopes of AGB and post-AGB stars. The properties of OH 1612 MHz maser emission from OH/IR stars at the tip of the AGB are the best understood.

Almost all OH 1612 MHz spectra show a double-peaked profile which is characteristic of maser emission from a thin spherical shell of a constant radius and expansion velocity. In an OH 1612 MHz survey of the Galactic Plane, Sevenster et al. (2001) found that 86% had double-peaked profiles, 13% had single-peaked profiles while less than 1% of sources had irregular profiles with more than two emission peaks. A high degree of spherical symmetry in OH/IR stars has also been confirmed from aperture synthesis observations of approximately 30 sources (e.g. Chapman & Cohen 1985; Welty, Fix & Mutel 1987).

The post-AGB stars occupy a short-lived transition stage between AGB and PN phases. Maser observations of post-AGB stars provide a means of investigating the onset and development of wind asymmetries. Most studies of maser emission from post-AGB stars have concentrated on sources with unusual maser properties. Aperture synthesis observations for a sample of 10 post-AGB stars with unusually high OH expansion velocities, for example, are consistent with bipolar outflows and enhanced equatorial densities (Zijlstra et al. 2001). It is apparent that for some sources, wind asymmetries are present during the early post-AGB stage where molecular material leftover from the AGB phase is still present. However, Sevenster (2002a,b) has argued that only a small fraction of both AGB and post-AGB sources have irregular OH 1612 MHz spectra.

To investigate the onset and incidence of wind asymmetries during the post-AGB phase, we are observing the maser properties of an OH-selected sample of 86 post-AGB stars with well-determined far-infrared properties. Here we present total intensity spectra obtained for the OH ground state maser transitions at 1612, 1665, 1667, and 1720 MHz and discuss their statistical properties. Other maser transitions and their polarisation properties will be discussed in future papers.

2. Sample Selection

We have selected a well-defined sample of 86 compact sources from the OH 1612 MHz survey of Sevenster et al. (1997a,b, 2001). This survey, taken with the Australia Telescope Compact Array (ATCA) and the Very Large Array (VLA) (hereafter the ATCA/VLA survey) detected OH 1612 MHz maser emission from a total of 766 compact sources. The OH 1612 MHz maser positions were measured with a precision of typically 0.5 arcsec and stellar velocities to 1 km s^{-1} . The survey is 95% complete for peak OH flux densities above 0.38 Jy.

Sevenster (2002a,b) compared the far-infrared IRAS (InfraRed Astronomical Satellite) and MSX (Mid-course Space Experiment) properties for sources in the ATCA/VLA survey

and has shown that the far-infrared colours provide a powerful tool for distinguishing between AGB and post-AGB stars. Figure 1 shows an IRAS two-colour diagram for 239 sources in the ATCA/VLA survey that have well-determined flux densities (quality flag 2 or 3) in the IRAS 12, 25, and 60 μm bands. The infrared colours are defined as $[a-b] = 2.5 \log (S_b/S_a)$ where S is the flux density in Jy and a, b , are wavelengths in μm . The solid line shows the well-known evolutionary track for AGB stars, defined by van der Veen & Habing (1988). The right-hand IRAS (RI) region has traditionally been associated with post-AGB stars that have evolved to the right of the evolutionary track. Increasing $[12-25]$ colour indicates thickening circumstellar shells. A second group of likely post-AGB stars, discussed by Sevenster (2002b), the left-hand IRAS (LI) group, lies to the left of the track. These stars have a 60 μm excess indicating large amounts of cool dust are around these stars, probably due to very high mass-loss rates. Sevenster has shown that this group contains stars with higher outflow velocities ($> 15 \text{ km s}^{-1}$) and higher initial masses. The RI and LI groups probably represent different evolutionary sequences for lower and higher mass post-AGB stars respectively with an initial mass separation between the two groups at $4 M_{\odot}$. The IRAS colours for the RI group are $[25-60] < 1.5$ and $[12-25] > 1.4$. For the LI region the IRAS colours are $[25-60] > -0.2$ and $[12-25] > 0.2$, with $[25-60] > -2.15 + 0.35 \exp(1.5 [12-25])$.

Figure 2 shows an MSX two-colour diagram for 424 sources in the ATCA/VLA survey with well-determined MSX flux densities in the 8, 12, 15, and 21 μm bands. Following Sevenster (2002a), the diagram is split into four quadrants separated at $[8-12] = 0.9$ and $[15-21] = 0.7$. The MSX colours provide a clear separation between AGB stars and post-AGB stars to the right of the IRAS evolutionary track. Early (younger) post-AGB stars are located in Quad IV and late (more evolved) post-AGB stars in Quad I. Quad II contains star-forming regions. Quad III includes both AGB stars and LI sources. The MSX colours for Quad IV stars are $[15-21] < 0.7$ and $[8-12] > 0.9$. For Quad I, the MSX colours are $[15-21] > 0.7$ and $[8-12] > 0.9$.

Our sample is the set of 88 sources in the ATCA/VLA survey with OH 1612 MHz detections and far-infrared colours corresponding either to the IRAS RI and LI groups or to MSX Quads I and IV. The number of sources in each group are: 38 RI, 30 LI, 15 Quad IV, and 24 Quad I. As shown in Figures 1 and 2 there is an overlap between the IRAS and MSX groups; 12 stars are both Quad I and RI objects, six are Quad IV and RI, and one source is a Quad IV and LI object. No objects are in both the Quad I and LI groups.

Table 1 lists the source parameters for the 88 sources. The columns give the source identifier from the ATCA/VLA survey (Sevenster et al. 1997a,b, 2001), IRAS Name, Right Ascension and Declination (J2000), radial velocity of the central star (relative to the Local

Standard of Rest), the IRAS 12, 25, and 60 μm and MSX 8, 12, 15, and 21 μm flux densities, and the classification/s of each source as RI, LI, Quad I, or Quad IV. All coordinates in this paper are given for the epoch J2000 unless otherwise stated. The radial velocities are from the ATCA/VLA survey and the infrared flux densities are reproduced from Sevenster (2002a,b). Two sources in Table 1, d29 (OH323.459-0.079, Chan, Henning & Schreyer 1996) and v280 (OH43.165-0.028, Caswell 2004) have previously been identified as star-formation regions and are not discussed further in this paper. Our final sample therefore consists of 86 sources.

3. Observations and Analysis

3.1. Parkes Observations

Observations were taken for the four ground-state OH maser transitions with rest frequencies of 1612.231, 1665.4018, 1667.359, and 1720.530 MHz, using the Parkes radio telescope in 2002 September, 2003 January/February, and 2003 August. A linear feed with a radio frequency hybrid was used to generate two circular polarisations. All observations were taken with the H-OH receiver, a bandwidth of 4 MHz, on-line Doppler tracking, and the Parkes multibeam correlator configured for 8192 channels. Only the central 2 MHz were recorded for 1612 MHz observations. At 18 cm the FWHM of the telescope primary beam is 12.6 arcmin. Table 2 lists the observing dates and frequencies, average integration times, and the typical 1σ noise per channel of spectra in each observing run. Severe dust storms around Parkes on 2003 January 30 are responsible for the anomalously high noise levels on this date.

Initial data reduction to calibrate the spectral bandpass and absolute flux scale was carried out using SPC, a single-dish spectral line reduction package supported by the Australia Telescope National Facility (ATNF). Absolute flux calibration was applied using observations of the standard sources Hydra A and 1934-638. Flux densities of 38.0 Jy (1612 MHz) and 37.0 Jy (1665/1667/1720 MHz) for Hydra A, and 15.0 Jy (1612 MHz) and 14.9 Jy (1665/1667/1720 MHz) for 1934-638 were assumed. Further data reduction involving Hanning-smoothing, baseline calibration, and flagging was carried out with the Spectral Line Analysis Package (SLAP, Staveley-Smith 1985), an interactive program for radio spectral line data reduction. The channel separation and velocity resolution of the spectra were 0.09 and 0.18 km s^{-1} respectively. All velocities are given in the radio convention with respect to the Local Standard of Rest.

The spectra were analysed using SLAP with peak flux densities and velocities measured for either one (for irregular or single-peaked sources) or two (for double-peaked sources)

emission peaks. Emission peaks were considered to be definite detections if one of the following criteria was satisfied:

- Peak flux density $> 5\sigma$ and linewidth > 10 channels (0.9 km s^{-1}); or
- Peak flux density $> 5\sigma$, linewidth = $6 \rightarrow 10$ channels and velocity consistent with emission feature detected in another OH transition; or
- Peak flux density $> 5\sigma$, linewidth = $4 \rightarrow 5$ channels and spectrum double-peaked with both peaks detected in another OH transition; or
- Peak flux density $3 \rightarrow 5\sigma$, linewidth > 10 channels and spectrum double-peaked with both peaks detected in another OH transition.

Occasionally the Parkes spectra are confused by other sources detected within the primary beam. In some cases, confusion can be attributed to nearby compact stellar maser sources with identifications in the ATCA/VLA survey. Confusion also arises from OH emission and absorption from extended gas clouds in the Galactic plane, particularly for sources with longitudes close to the Galactic centre. This type of confusion is characterised by broad emission and/or absorption ($> 10 \text{ km s}^{-1}$) with features often being present at the same velocities at all four frequencies (Haynes & Caswell 1977).

3.2. Australia Telescope Compact Array Observations

Observations at 1720 MHz were taken with the EW367 array configuration with all six antennas of the ATCA on 2003 August 8, for 18 sources with 1720 MHz emission detected within the beam of the Parkes telescope. The ATCA is an array of six 22-m diameter dishes that are located on an east-west track, with a maximum baseline of 6 km (Frater, Brooks & Whiteoak 1992). Each source was observed in seven two-minute cuts distributed over an eight-hour observing period. A bandwidth of 4 MHz was used with 1024 channels, giving a channel separation of 0.73 km s^{-1} and a velocity resolution of 0.88 km s^{-1} . The data were reduced using the Miriad reduction package (Sault, Teuben & Wright 1995). To search for compact sources, images were made using natural weighting with an angular resolution of typically $6'' \times 14''$, measured east-west by north-south.

On 2003 July 23/24 and 2003 August 7, observations of the 1665 and 1667 MHz OH transitions were taken at the ATCA. Each source was observed for typically eight two-minute cuts, distributed over a 12 hour period. The two OH mainlines were observed simultaneously

using a 4 MHz bandwidth with 1024 spectral channels. The channel separation is 0.70 km s^{-1} and the velocity resolution is 0.84 km s^{-1} . The 6D array was used, giving an angular resolution of approximately $7'' \times 10''$. Table 2 gives the observing dates and frequencies, average integration times, and the typical 1σ noise per channel (measured in line-free channels) for the ATCA observations.

The ATCA OH mainline spectra are not shown but have been used to confirm maser positions and to verify whether the OH mainline detections obtained from the Parkes data are associated with the stellar sources, or are due to sources of confusion or interference. As an example, Figure 3 shows the Parkes and ATCA spectra of b292 at 1720 MHz plotted over the same velocity range. The features detected with the Parkes radio telescope at velocities below 60 km s^{-1} are completely absent in the ATCA spectrum confirming that these are due to Galactic plane confusion. The 1720 MHz emission from b292 is discussed further in Section 5.

4. Results

4.1. OH 1612, 1665 and 1667 MHz detections

All 86 sources selected from the Sevenster survey were re-detected at 1612 MHz with the Parkes telescope. Of the 86 sources, 27 (31%) were detected at 1665 MHz and 45 (52 %) were detected at 1667 MHz. The maser detections are summarized in Table 3. The three rows for each source give the 1612, 1665, and 1667 MHz results respectively. The columns are:

- 1: source name, as given in the ATCA/VLA survey;
- 2–4: velocity, peak flux density and integrated flux density for the blue-shifted emission peak of double-peaked sources, or for the strongest emission peak from sources with single peaks or irregular spectra;
- 5–7: velocity, peak flux density and integrated flux density for the red-shifted emission peak;
- 8: peak-to-peak flux density ratio;
- 9: integrated flux density ratio
- 10: total velocity range of detected emission (excluding absorption and identified confusion)

- 11: spectral classification (explained in Section 6.1)
- 12: Variability, marginal detection and date flag: A ‘V’ in this column indicates the peak flux of a source at 1612 MHz is more than 30 % variable (see Section 6.4). An ‘m’ in this column indicates that the detection was marginal with a peak flux density of $3 \rightarrow 5$ sigma. Marginal detections are included in Figure 7 but are not included in source counts and further discussion. A ‘#’ indicates that the observation was taken on 2003 August 18. All other Parkes data for the 1612, 1665, and 1667 transitions were taken in 2003 September.

The Parkes spectra are plotted in Figure 7 with labels in the top-left and top-right corners giving the source name and OH transition respectively. OH emission peaks from nearby sources are indicated where these have been identified.

4.2. Notes on individual sources

The following notes refer to the OH 1612, 1665, and 1667 MHz Parkes spectra shown in Figure 7.

d3: Confusion from d2 at 1612 MHz.

d34: Confusion from d33 at 1612 MHz.

d46/d47: These two sources suffer mutual confusion as well as from Galactic dust clouds. Absorption at -20 and -50 km s $^{-1}$ is evident in the mainline spectra of both sources (off-scale in the figure for d46). The 1720 MHz line is seen at these velocities in absorption in d46 and in emission in d47, and there is 1612 MHz absorption at -20 km s $^{-1}$ in d47. These features are attributed to the same network of Galactic dust clouds. The strongest 1612 MHz peaks in d47 appear faintly in the d46 spectrum (outside range shown in figure).

d47 is the only source with a strong, symmetrical four-peaked OH 1612-MHz profile. ATCA observations confirm that the narrow emission peaks in the mainline spectra at -30 and -70 km s $^{-1}$ are associated with the stellar source. The ATCA observations detected several weak 1667 MHz emission features between -30 and -74 km s $^{-1}$, including one at 50 km s $^{-1}$, which was detected at Parkes but confused with an absorption dip at that velocity.

d62: Confusion from d59 at 1612 MHz. The mainline features seen in the Parkes spectra may include some background Galactic confusion and variable features.

d93: The weak 1612 MHz peaks at -117.1 and -39.5 km s $^{-1}$ are likely to be radio frequency interference (RFI).

b11: The stellar velocity is revised to 13.4 km s^{-1} , from the velocity of 25.3 km s^{-1} given by Sevenster et al. (1997a) as the new observations show a double-peaked 1667 MHz spectral profile and broad 1665 MHz emission centred at this velocity.

b14: The peak at 50.4 km s^{-1} at 1612 MHz is not present in the ATCA/VLA spectrum and is attributed to an unknown confusing source. There is no match with any other ATCA/VLA sources. It does not have a typical signature of RFI.

d200: The stellar velocity has been revised to -74.7 km s^{-1} for this source on the basis of its double-peaked 1612 MHz profile.

b25: A small broad peak at -40 km s^{-1} at 1612 MHz is attributed to Galactic confusion, as it is not present in the ATCA/VLA spectrum.

b33: This source has four peaks at 1612 MHz. The peak at -4 km s^{-1} is too narrow (3 channels) to be a reliable detection. The peaks at -36 and -12 km s^{-1} were identified with this source in the ATCA/VLA survey. The peak at -21 km s^{-1} may be from a confusing source, as there is absorption near this velocity.

b44: This source shows one definite peak at -35.0 km s^{-1} at 1612 MHz and a weak narrow peak at -9.5 km s^{-1} that is probably RFI. A second peak at $+30.5 \text{ km s}^{-1}$ noted in the ATCA/VLA survey was not detected here.

b62: This is an irregular source at 1612 MHz with three peaks apparent. It is possible one or more emission features are due to extended Galactic emission as there is absorption at a nearby velocity (5 km s^{-1}). The two narrow spikes at -9 and -3 km s^{-1} in the 1612 MHz spectrum are likely to be RFI.

b96: This source shows four peaks at 1612 MHz. The peaks at -127 and -146 km s^{-1} were identified in the ATCA/VLA survey. The peaks at -118 and -136 km s^{-1} have not been identified with another source. Higher resolution observations are needed to determine if the latter peaks are associated with b96.

b133: The narrow peaks at -2 and -8 km s^{-1} are likely to be RFI. The broader peaks at 18 and -24 km s^{-1} were identified in the ATCA/VLA survey.

b155: There is probable RFI at -13.5 km s^{-1} at 1612 MHz.

b199: The drop-off at the red-shifted end of the baseline in both spectra is due to a poor baseline fit to complex absorption features in the spectrum.

b246: The stellar velocity has been revised to 138.0 km s^{-1} from the central velocity of the 1612 and 1665 MHz spectra

b292: This source is the only post-AGB object previously detected at 1720 MHz (Sevener & Chapman 2001) and the only source detected in the present study where the 1720 MHz emission is associated with the stellar source (see Section 5). As shown in Figure 3, Galactic confusion was detected at velocities of -20 , 20 , and 40 km s^{-1} .

b301: Confusion from b298 at 1612 MHz.

b304: This source has probable RFI at -5.0 km s^{-1} at 1612 MHz .

v50: This source has probable RFI at -5 km s^{-1} at 1612 MHz, and at 5 , 95 , and 100 km s^{-1} at 1667 MHz.

v53: Galactic confusion is present in the Parkes observations. ATCA observations at 1667 MHz confirmed only a narrow peak near 4 km s^{-1} , similar in width to the 1612 MHz peaks and much narrower than the 1667 MHz Parkes spectrum, leading to a 1667 MHz classification as S rather than I (see Section 6.1).

v117: The Parkes 1667-MHz spectrum shows confusion at velocities above 70 km s^{-1} . The ATCA observations confirm that the broad emission peak seen at all three frequencies around $40\text{-}50 \text{ km s}^{-1}$ is associated with the stellar source.

v154: Confusion from v156 at 1612 MHz.

v162: Confusion from v158 at 1612 MHz. The two narrow peaks at 86.6 and 89.1 km s^{-1} are probably RFI.

v268: This source has an unidentified peak at 21 km s^{-1} , likely to be RFI or confusion from interstellar clouds. There is also RFI at 6 km s^{-1} and weakly at velocities above 90 km s^{-1} .

v270: There is probable RFI at 60 , 115 , and 135 km s^{-1} at 1667 MHz.

5. OH 1720 MHz results

From the Parkes observations, a total of 18 sources showed 1720 MHz emission features. In most cases the emission was broad and coincident in velocity with other features detected in the OH mainlines that were known to be from unrelated Galactic emission. These sources were not detected in the follow-up ATCA 1720 MHz observations, confirming that the emission was spatially extended.

For three sources, the ATCA images showed compact sources of 1720 MHz emission within 20 arcmin of the stellar position. For d168, the ATCA 1720 MHz maser position,

determined to a precision of approximately one arcsec, is $17^h5^m11.3^s$, $-41^\circ28'44''$, offset by ~ 15 arcmin from the stellar position. The 1720 MHz detection is probably associated with the star-formation region IRAS 17016-4124, also known as G345.0-0.2 ($17^h1^m40.268^s$, $-41^\circ25'01.16''$ (B1950), Gaume & Mutel 1987).

For b33, the position of the compact 1720 MHz source is $17^h25^m32.4^s$, $-36^\circ21'51''$, offset by 8 arcmin from the stellar position. This is clearly associated with IRAS 17221-3619 ($17^h25^m31.7^s$, $-36^\circ21'54''$), a massive young stellar object (Chan et al. 1996).

For b292 (OH009.1-0.4) the ATCA 1720 MHz observations confirm the presence of a compact maser source associated with the stellar source, previously reported by Sevenster & Chapman (2001). The ATCA 1720 MHz position is $18^h7^m20.9^s$, $-21^\circ16'10.9''$, in excellent agreement with the OH 1612 MHz maser position (see Table 1) and with the previously published 1720 MHz position from Sevenster & Chapman (2001).

Figure 3 shows the 1720 MHz Parkes and ATCA spectra for b292 obtained in February 2003 and August 2003 respectively. The Parkes spectrum shows a narrow emission feature with a peak flux density of 2.0 Jy at a velocity of 69.2 km s^{-1} , consistent with the previous detection at ATCA of an emission peak of 1.22 Jy at a velocity of 69.4 km s^{-1} reported by Sevenster & Chapman (2001). The lower velocity resolution of this previous observation accounts for the lower peak flux.

From the MSX colours, b292 is a likely young post-AGB star. It is unusual among our sample in that it has 1665 MHz emission but no 1667 MHz emission (see Sections 4.1 and 6.3). Figure 5 (top) shows the 2002/2003 Parkes spectra at 1612, 1665, and 1720 MHz. The strongest emission, at 1612 MHz, is one sided with a blue-shifted peak of 18.9 Jy at 70.4 km s^{-1} . A much weaker red-shifted peak was detected at velocities near 99 km s^{-1} but is not seen in Figure 5 as scaling has reduced the feature to insignificance. The 1665 MHz emission is also strongest at blue-shifted velocities with a peak flux density of 7.4 Jy at 69.7 km s^{-1} . We detected a second weaker 1665 MHz peak with a flux density of 1.6 Jy at a velocity of 104.0 km s^{-1} that was not evident in the 1998 observations of Sevenster & Chapman. From the double-peaked 1665 MHz spectrum we obtain an expansion velocity at 1665 MHz of 17.1 km s^{-1} and a stellar velocity of 87.0 km s^{-1} . As previously reported, the narrow 1720 MHz emission peak is seen at a slightly more blue-shifted velocity than the bluest 1612 and 1665 MHz emission peaks.

A comparison of our spectra with the previous spectra from Sevenster & Chapman (2001) indicates negligible variability in the 1720 and 1612 MHz emission between 1999 and 2003. However, a comparison of the 2003 ATCA 1665 MHz spectrum with the earlier spectrum, obtained with the same velocity resolution of 0.8 km s^{-1} , shows that the 1665

MHz emission has increased significantly in intensity, from a peak flux density of 1.64 Jy in 1998/1999 to a peak flux density of 2.2 Jy in 2003 July.

The physical conditions needed for 1720 MHz maser emission have been tightly constrained by modelling (Lockett, Gauthier & Elitzur 1999; Elitzur 1976). Temperatures of 50–125 K, densities around 10^5 cm^{-3} , and OH column densities of order 10^{16} cm^{-2} are required. 1720 MHz masers are thought to be shock excited, rather than radiatively pumped and a theoretical explanation of their production, based on the formation of C-shocks in a molecular cloud is given by Wardle (1999). In addition, the masers are strongly beamed (see below). In circumstellar shells, the likely mechanism leading to the creation of a C-type shock is the interaction of the fast post-AGB wind with the remnant slow AGB wind (Sevenster & Chapman 2001), with the 1720 MHz maser being produced in the interaction zone. This is a similar mechanism to the production of 1720 MHz masers in supernovae remnants (Frail, Goss & Slysh 1994).

Sevenster & Chapman (2001) previously predicted that H_2O maser emission would *not* be present in b292 since the passage of a C-type shock would not lead to a sufficiently strong increase in the density of H_2O (Wardle 1999). However for b292 we *have* detected H_2O maser emission. Figure 5 (bottom) shows a 22 GHz spectrum obtained from an ATCA observation on 2002 September 24 by Deacon. Three peaks were detected. As this was a “snap-shot” observation it could not be confirmed that the H_2O emission was from the stellar position, but an association is probable as the velocity range of the H_2O emission is similar to that of the OH emission (between 72 and 106 km s^{-1}) and there are no known other maser sources within the $2.75' \text{ 22 GHz ATCA beam}$.

The presence of H_2O and 1612 MHz OH maser emission in addition to the shock excited 1720 MHz emission implies a strong variation in the properties of the mass outflow from b292 since the 1612 and H_2O masers cannot be spatially co-located within the circumstellar envelope with the 1720 MHz maser emission. We predict that the OH 1665 and 1612 MHz and most blue- and red-shifted H_2O maser emission arises from the remnant AGB wind while the OH 1720 MHz emission is in a new bipolar outflow that is starting to disrupt the spherical AGB shell (giving a De profile at 1612 MHz - see Section 6.1). This stream could indicate a high-speed collimated outflow of the type proposed by Sahai & Trauger (1998). If the outflow is not parallel to the line of sight, the 1720 MHz velocity is seen in projection. The central H_2O emission probably arises quite close to the central star.

Our detection rate for 1720 MHz maser emission from post-AGB stars of $1/86$ indicates that the conditions for 1720 MHz emission are rarely met and/or the time period for occurrence is very short. One factor decreasing the detection rate is that the maser emission is beamed parallel to the C-shock front and is tangentially amplified. This requires that

the shock must be near-perpendicular to the line-of-sight for maser emission to be observed (Wardle 1999). 1720 MHz masers are also very dependent on physical conditions. Higher densities first quench the 1720 MHz masers, then favour production of 1612 MHz masers while higher temperatures favour the formation of mainline masers (Lockett et al. 1999). As discussed in Section 6, bipolar outflows in post-AGB stars are usually traced by mainline and 1612 MHz OH emission. Given the unusual physical conditions required, the low detection rate for 1720 MHz maser emission in post-AGB stars is not surprising.

6. Discussion

6.1. Spectral Profile Classifications

In this section we discuss the maser properties of the OH 1612, 1665, and 1667 MHz transitions. Table 4 summarises the number of OH detections at 1612, 1665, and 1667 MHz by frequency and, using a profile classification scheme, spectral profile. All 86 sources were detected at 1612 MHz while OH mainline emission was detected in one or both of the OH mainline transitions from a total of 50 sources. 23 sources were detected at 1667 MHz only, five sources were detected at 1665 MHz only, and 22 sources were detected in both mainlines. For 81/86 sources the OH 1612 MHz transition is the strongest while for sources detected in both 1665 and 1667 MHz the 1667 MHz transition almost always dominates. In many cases the 1667 MHz profiles are very similar (though weaker) to the OH 1612 MHz spectra while the weaker OH 1665 MHz transition may show a different profile type. Two examples of sources which differ from this are d46, where the strongest emission occurs at 1665 MHz, and b11 where the OH 1667 MHz emission is considerably stronger than the 1612 MHz emission.

We have identified six different types of spectral profiles. The majority of our sources have double-peaked profiles at one or more of the OH maser transitions, but distinct variations on this ‘classic’ profile have been recognised along with single-peaked and irregular spectra. The six categories are listed and described below. Figure 6 shows an example spectrum for each of the six categories.

- **D:** ‘Double’ - Double-peaked profiles with peak-peak flux density ratios < 8.0 . This is the “classic” profile type associated with OH/IR stars on the AGB. In our sample of likely post-AGB stars this is the most common profile type for both the 1612 and 1667 MHz transitions. Approximately 70% of the OH 1612 MHz spectra, and 50% of OH 1667 MHz spectra, have D-type profiles. At 1665 MHz the incidence of D-type profiles is considerably lower (19%).

- **De:** ‘Double extreme’ - Profiles with peak-peak flux density ratios > 8.0 . There is a large population of sources with peak-to-peak ratios of 3 or less, and a small population with much larger ratios. A cutoff of 8.0 separates these two groups cleanly. Four sources (d200, b134, b292, and v223) have De profiles at 1612 MHz while two sources (v67 and v132) have De profiles at 1667 MHz.

It appears likely that De maser profiles originate from OH shells that are still largely spherical, rather than from bipolar outflows. The OH spectral profiles at other transitions for the De sources are mostly D-type indicating spherical maser shells. For v132, MERLIN images at 1612 and 1667 MHz show little evidence for an aspherical maser shell (Bains et al. 2003).

There are several possible causes for a De-type spectrum: An asymmetric external UV field (responsible for dissociating H_2O to OH) may lead to OH emission that is stronger on one side of the star. Localised turbulence, possibly from the onset of bipolar outflows could disrupt the velocity coherence needed for maser emission. In sources with weak red-shifted emission, the maser emission from the far side of the circumstellar envelope may be absorbed in an ionised region near the star (Zijlstra et al. 2001).

- **Dw:** ‘Double with wings’ - Double-peaked profiles with sloping outer edges rather than the near-vertical outer edge of D-type sources. Four sources in our sample, b70, b112, v41, and v274, have this profile type for one or more lines. A well-known example of a Dw source is HD101584 at 1667 MHz. Other examples are IRAS 17253-2831 at 1612 MHz, IRAS 18491-0207 at 1667 MHz, and IRAS 22036+5306 at 1612, 1665, and 1667 MHz. Interferometric observations of these sources reveal the masers are located in bipolar outflows, with the blue- and red-shifted masers on opposite sides of the central star (Zijlstra et al. 2001). At other OH transitions these sources mostly have irregular profiles.
- **DD:** ‘Double-double’ - One source in our sample, d47, shows four emission peaks at 1612 MHz, symmetrical in outflow velocity and strength around the central stellar velocity. The OH/IR star OH19.2-1.0, is known to have a similar OH profile (Chapman 1988) at 1612 MHz. In her model for this star, based on interferometric observations of the maser positions, Chapman proposed that the masers are located on two rings that are the cross-sections of two bipolar cones of emission expanding at terminal velocity. This model predicts the two outer peaks in the maser spectrum to be the strongest. However, for d47 the strongest emission occurs from the two inner peaks. A plausible explanation for the stronger inner peaks, based on the Chapman model, is that the masers are located in regions where the outflows are accelerating.

The distinctiveness of this spectral profile and the previously-substantiated interpretation from the literature, warrants the DD category even though our sample contains only a single example. It is possible that other sources in this sample, particularly those with Dw or multiple-peaked irregular profiles, have a DD profile too faint to detect.

- **S:** ‘Single’ - Single-peaked profiles with one narrow emission peak with a steep edge on one side of the feature. Our sample includes 10 sources with an S-type profile at 1667 MHz. Of these nine sources have a D- or De-type profile in the stronger 1612 MHz transition. This indicates that most S-type sources are intrinsically double-peaked with one peak below the detection level. A few sources (e.g. b11) have strong single peaks indicating that some S profiles are intrinsically De sources. There is no distinct grouping in infrared colour, or preference for the red- or blue-shifted peak being absent.
- **I:** ‘Irregular’ - These profiles exhibit a range of features that include one wide peak, several peaks, or plateaus of emission with peaks superimposed. The complex, multiple-peaked spectra, such as d46, with large velocity widths almost certainly have bipolar outflows and a remnant AGB wind still present. Several examples are discussed in Zijlstra et al. (2001). The OH 1667 MHz emission from v231 is a good example of an irregular profile showing elements of two emission peaks (indicating a remnant spherical AGB shell), high-velocity emission (linear bipolar outflow), and central-velocity emission plateau (inner accelerating outflow).

16/27 of the OH 1665 MHz detections show I-type profiles. For nine of these sources, the 1665 MHz spectra have multiple peaks while the 1612 MHz spectra have an I, DD, or Dw classification at 1612 MHz, consistent with aspherical morphologies. For four sources (d93, d189, b258, and v45) the 1665 MHz emission shows a broad single feature that is centred on the stellar velocity while the 1612 MHz emission is double-peaked and wider than the 1665 MHz feature. For these sources the circumstellar envelopes are likely to be spherically symmetric with the 1665 MHz emission occurring in an inner accelerating region where the logarithmic velocity gradient is > 1 (Chapman & Cohen 1985). For the remaining three sources (b11, v67, and v237) irregularities in the 1665-MHz spectra indicate some degree of asymmetry in the 1665 MHz outflows although the 1612 MHz emission is double-peaked.

In summary, we consider that the D-, De-, and S-type profiles indicate spherical maser morphologies while the Dw-, DD-, and I-type profiles indicate circumstellar shells with some asymmetries. Based on these two groups, 18/86 sources show some degree of asymmetry at 1612 MHz. An additional three sources show irregularities at 1665 MHz and one source

(d168) appears irregular at 1667 MHz only. Taken together, 22/86 (25 %) sources in our sample show signs of aspherical morphologies.

6.2. OH 1667 MHz Overshoot

All but eight sources have velocity ranges $< 50 \text{ km s}^{-1}$ (measured at a cut-off level of 3σ). The largest velocity range of 78 km s^{-1} is observed for v231 at 1667 MHz. The average velocity ranges are 34.6 km s^{-1} at 1612 MHz, 28.9 km s^{-1} at 1665 MHz, and 34.8 km s^{-1} at 1667 MHz.

For sources detected at both 1612 and 1667 MHz, 30 out of 35 have a larger velocity range at 1667 MHz than at 1612 MHz (excluding single-peaked sources). For these sources the 1667 MHz velocity range is up to 18 km s^{-1} larger than at 1612 MHz with an average difference of 1.5 km s^{-1} , corresponding to 16 spectral channels.

For *all* sources with double-peaked spectra at both 1612 and 1667 MHz (24) the velocity range at 1667 MHz is the same or larger than at 1612 MHz. The largest difference is 5 km s^{-1} and the average is 2.3 km s^{-1} . A 1667 MHz overshoot is also evident in the peak velocities. In most cases both the blue- and red-shifted peaks at 1667 MHz are outside the 1612 MHz peaks. The largest peak shift is 7 km s^{-1} with an average of 0.78 km s^{-1} , corresponding to 9 spectral channels.

It is clear that 1667 MHz masers regularly overshoot 1612 MHz masers in both spherical and irregular envelopes. These results are very similar to Sivagnanam & David (1999) in a study of the overshoot of mainline spectral extent in circumstellar OH masers. Their sample included 21 AGB and post-AGB stars. Our results come from a much larger sample size confirming that the phenomenon is real.

Sivagnanam & David (1999) suggested several possible mechanisms for this effect including Zeeman broadening of the 1667 MHz line, clumping in the stellar envelope, velocity fluctuations affecting 1612 MHz maser coherence, or axisymmetric winds. One possibility is that some acceleration is still present at large radii where OH 1612 and 1667 MHz masers exist, and the distances at which the 1667 MHz masers are located extends further than for 1612 MHz masers. This is the case for the supergiant star, IRC+10420 and HD 179821, which may be a supergiant or a post-AGB star (Bowers 1984; Gledhill, Yates & Richards 2001). Both of these stars have spherical, although somewhat clumpy and distorted, circumstellar OH shells that give De-type spectral profiles. In IRC+10420 the 1612 MHz masers are located between 3000 and 11000 AU but the 1667 MHz masers extend to 18000 AU. There is a velocity gradient of about 2 km s^{-1} between the 1612 and 1667 MHz shells which

affects the velocity range of the spectral profiles: the 1667 MHz spectral width is larger than the 1612 MHz spectral width by 4-5 km s⁻¹. In two other supergiants, VX Sgr and VY CMA, velocity gradients exist to large radii (Chapman & Cohen 1986; Reid & Muhleman 1978). However, in these two stars the OH 1667 MHz masers are located inside the OH 1612 MHz shell. One other supergiant, NML Cyg, has inner circumstellar regions that appear to be expanding *faster* than the outer regions (Diamond, Norris & Booth 1984). In some Mira variables there is evidence for velocity gradients to large radii in spherical circumstellar shells, e.g. in U Her and R Cas (Chapman et. al. 1994). Two OH/IR stars imaged (OH127.8-0.0 and OH26.5+0.6) have small upper limits on possible velocity gradients in their 1612 MHz shells (Bowers & Johnston 1990).

Imaging of v132 by Bains et al. (2003) reveals that the D-type 1612 MHz masers are contained in an ellipse with inner radius 250 mas and outer radius 650 mas, and the De-type 1667 MHz masers trace a thinner ellipse extending to a radius of 850 mas. However, the velocity range at each line is very similar and there is no evidence of a velocity gradient at large radii.

It is apparent that there are a range of characteristics of the 1667 and 1612 MHz OH masers in late-type stars. In explaining the 1667 MHz overshoot phenomenon for sources with double-peaked spectra at both 1612 and 1667 MHz, a mechanism that simply broadens 1667 MHz emission in the standard maser envelope model may be possible but it is likely that the 1667 MHz masers are often located at radii beyond the 1612 MHz masers.

6.3. IRAS and MSX Colours

Table 5 summarises the number of detections for each OH maser transition for the four groups used in the infrared selection criteria discussed in Section 2, namely the IRAS LI and RI groups, the MSX Quad IV (early post-AGB) and Quad I (late post-AGB) groups. As previously described there is an overlap between these groups. The IRAS LI sources correspond to MSX Quad III while the RI sources correspond to MSX Quads I and IV. IRAS and MSX colour-colour plots of sources detected at 1612, 1665, and 1667 MHz are plotted in Figure 4, combining graphically the results in Tables 4 and 5.

Figure 4 shows that for both LI and RI regions and both MSX Quads 1 & IV, the majority of sources have double-peaked (D-type) profiles, at 1612 MHz. In detail, 13 of the 15 early post-AGB stars (Quad IV) have D-type spectra while the other two sources have De-type spectra. We therefore find no evidence for strongly disturbed outflows in the early post-AGB region. In contrast, for the late post-AGB stars (Quad I), eight out of 22 sources

have I- or Dw-type profiles at 1612 MHz. Based on this sample we therefore estimate that approximately one-third of post-AGB stars develop aspherical morphologies during the late post-AGB stage.

The location on the colour-colour plots of the I- and Dw-type sources indicates a progression with the maser profiles of some sources evolving from a spherical outflow with a D-type spectrum, to a disturbed outflow with an I-type spectrum, and finally in some cases to a fully bipolar outflow and Dw-type spectrum. Both the IRAS and MSX diagrams show that the Dw sources have the most extreme far-infrared colours with $[12-25] > 2.3$ and $[15-21] > 1.5$. This progression can be seen at both 1612 and 1667 MHz as the 1667 MHz spectral characteristics largely mirror those at 1612 MHz. The small number of sources with De-type profiles may come from an intermediate stage in some cases between the D and I profile types that occurs when a spherical outflow is first disturbed by a jet outflow as proposed by Sahai & Trauger (1998).

The OH 1665 MHz emission is the weakest of the three transitions and is detected most frequently from sources with irregular outflows. Of the 60 sources with double-peaked profiles at 1612 MHz, only 12 were detected at 1665 MHz whereas for 13 sources with irregular 1612 MHz spectra, eight were detected at 1665 MHz. In several late-type stars it has been found that 1665 MHz masers are located closer to the central star than 1612 and/or 1667 MHz masers. For example, in images of VX Sgr (Chapman & Cohen 1986), Roberts 22 and IRAS 18491-0207 (Zijlstra et al. 2001), and U Ori (Chapman, Cohen & Saikia 1991). The irregular profiles could indicate the beginnings of bipolar outflows disrupting the inner masers, and/or it could reflect the clumpy nature of the maser distribution. Possibly for the 1665 MHz profiles showing a broad hump centred on the stellar velocity, they are from an inner accelerating outflow (see Section 6.1). All this implies that the 1665 MHz transition is likely to be a good tracer of the inner envelope, where early departures from spherical symmetry are seen. 1665 or 1667 MHz emission can dominate in sources with highly irregular outflows. Four out of the five objects with strongest emission at 1665 or 1667 MHz (d46, b11, b262, and b263) are late post-AGB objects with irregular profiles at one or more OH maser lines. (v189, an LI object with S-type spectra, is the exception.)

Our sample includes a total of 30 LI sources. As discussed by Sevenster (2002b) this group of sources are likely to have higher initial stellar masses and AGB mass-loss rates than the RI sources. The average outflow velocity (half the peak-to-peak velocity width) of the LI sources is 18.25 km s^{-1} , compared to 13.00 km s^{-1} for RI sources. This is close to the outflow velocities from stars with initial masses of 1.6 and $\sim 4 M_{\odot}$ as calculated by van der Veen (1989) and quoted by Sevenster (2002b), and supports the theory that the LI sources are more massive stars than those in the RI category. The post-AGB evolutionary track

(van Hoof, Oudmaijer & Waters 1997) highlighted by Sevenster (2002b) for LI stars passes through this section of the IRAS [12-25]/[25-60] diagram before looping up to higher [25-60] colour. The LI region overlaps with the AGB and may include some stars that are still in the AGB evolutionary phase. Sevenster (2002b) has proposed that the LI stars are likely precursors to bipolar planetary nebulae although this is not confirmed. Of the 30 sources at 1612 MHz, 26 have double- or weak single-peaked profiles indicating that their circumstellar envelopes are still fairly homogeneous. Two sources (d62 and b165) have irregular profiles, one (d200) is a De source and one (d47) is a DD source with four emission peaks. 14 LI sources were detected at 1667 MHz. These are located close to the AGB evolutionary track. A remarkable observational result is that only one LI source was detected at 1665 MHz while the ‘extreme’ LI region away from the evolutionary track is devoid of OH mainline maser emission. For the small region defined by the IRAS colours [12-25] > 0.75 and [25-60] < 0.7 there is a 100% detection rate for 1667 MHz maser emission. This group of sources are likely to be the youngest LI objects and may indeed still be AGB stars as they are located near the AGB evolutionary track at the point where the RI and LI sources diverge.

6.4. OH 1612 MHz Variability

As an indicator of OH 1612 MHz variability we have compared the peak flux densities from our Parkes data, taken in 2002–2003 with a velocity resolution of 0.2 km s^{-1} , with the ATCA/VLA survey peak flux densities, obtained in 1993–1995 with much lower velocity resolution of 1.5 and 2.3 km s^{-1} (Sevenster et al. 1997a,b, 2001). To compare the two sets of data obtained with different velocity resolution, the Parkes data were smoothed using a Gaussian smoothing function to approximately the same velocity resolution as the ATCA/VLA data. After smoothing, the average peak flux densities of the Parkes spectra were a factor of 1.3 times greater than for the ATCA/VLA spectra. The reason for this discrepancy is unclear but we assume that this is a systematic bias and not an effect intrinsic to the sources.

Overall, for 26 of the 86 sources in our sample (30%), the OH 1612 MHz peak flux densities measured in 1993–1995 differ by at least 30% from those measured in 2002–2003 (after smoothing and removing the bias). These likely variable sources are indicated in Table 3 by a ‘V’ in the last column. For 16 of the 26 sources the flux densities differ by at least 50%. In all cases the profile shapes are unchanged. We find no obvious correlations between variability and the profile type or infrared colours.

OH 1612 MHz variability is well understood for AGB stars but is poorly understood for post-AGB stars. For AGB stars, the OH 1612 MHz maser emission is strongly saturated and

radiatively coupled to the stellar pulsation cycle. The peak OH 1612 MHz maser emission typically varies in intensity, over the stellar light cycle, by a factor of two. Monitoring studies have shown OH light curves with periods from several hundred to several thousand days (e.g. Herman & Habing 1985; van Langevelde, van der Heiden & van Schooneveld 1990; Chapman, Habing & Killeen 1995).

It is often assumed that post-AGB stars are non-variable at 1612 MHz since for post-AGB stars the stellar pulsations are expected to have ceased. The comparison of the Parkes data with the earlier ATCA/VLA data shows that while the 1612 MHz variability *is* much weaker during the post-AGB phase, some variability is present for at least one-third of the sources in our sample. Monitoring data are needed to determine variability timescales and whether the 1612 MHz variability during the post-AGB phase is associated with (weak) stellar pulsations and/or with other mechanisms such as structural changes in the inner envelopes.

OH mainline variability will be discussed further in a later paper. Here we note that in at least some sources, strong 1665 MHz variability is present. As an example, for d47 the Parkes data taken (by us) in 2002 September and 2003 August show that the peak 1665 MHz flux density increased from 0.94 Jy to 7.74 Jy.

7. Conclusions

The results of an extensive multi-transition OH maser survey of 86 post-AGB stars have been presented. Selected from an OH 1612 MHz survey of the Galactic Plane, most sources are also strongest at 1612 MHz and have double-peaked profiles. All 86 sources were re-detected at 1612 MHz, 27 were detected at 1665 MHz and 45 at 1667 MHz. One source previously detected at 1720 MHz (b292) was re-detected.

A classification scheme is used to distinguish six profile types found. 22 sources in the sample have spectral profiles that indicate aspherical and/or bipolar outflows. There are signs of an evolutionary trend in the OH maser profiles of the lower-mass stars (56) in the sample. A fraction of sources with double-peaked profiles will evolve to irregular profiles (associated with bipolar outflows and remnant spherical shells), and then to winged double-peaked profiles indicative of fully-bipolar outflows.

A significantly higher percentage of aspherical post-AGB sources have 1665 MHz emission than spherical sources. 1665 MHz emission may be a good tracer of initial departures from spherical morphology in inner circumstellar envelopes. Highly irregular, late post-AGB sources also tend to be dominant at one of the mainlines rather than at 1612 MHz.

The more massive and bluer post-AGB stars, known as ‘LI’ sources, are thought to evolve into bipolar PN. This distinctive group are noteworthy in our sample in having mostly double-peaked profiles. They also show an almost complete lack of mainline emission, except in the youngest sources. The outflow velocities of the LI sources are on average 10 km s^{-1} larger than those of the redder ‘RI’ objects, supporting their probable higher initial mass status.

At least 30% of sources show variability at 1612 MHz, showing that some maser variability is still present in many post-AGB stars. The degree of variability is significantly smaller than in AGB stars.

Most sources with 1612 and 1667 MHz emission have broader emission at 1667 MHz. This overshoot phenomenon has been previously noted by Sivagnanam & David (1999). The origin of this effect is unclear but it appears likely that in many cases the 1667 MHz masers are found out to distances beyond the 1612 MHz masers in regions where small velocity gradients are still present in the outer radii of circumstellar envelopes.

ACKNOWLEDGEMENTS

We wish to thank Jim Caswell for many helpful discussions, and Aidan Hotan for observing assistance at Parkes in August 2003.

REFERENCES

- Bains, I., Gledhill, T. M., Yates, J. A., & Richards, A. M. S. 2003, MNRAS, 338, 287
- Bowers, P. F., & Johnston, K. J. 1990, ApJ, 354, 676
- Bowers, P. F. 1984, ApJ, 279, 350
- Bujarrabal, V., Guibert, J., Nguyen-Q-Rieu, & Omont, A. 1980, A&A, 84, 311
- Caswell, J. L. 2004, MNRAS, 349, 99
- Chan, S. J., Henning, T., & Schreyer, K. 1996, A&AS, 115, 285
- Chapman, J. M. 1988, MNRAS, 230, 415
- Chapman, J. M., & Cohen, R. J. 1985, MNRAS, 212, 375
- Chapman, J. M., & Cohen, R. J. 1986, MNRAS, 220, 513
- Chapman, J. M., Cohen, R. J., & Saikia, D. J. 1991, MNRAS, 249, 227
- Chapman, J. M., Habing, H. J., & Killeen, N. E. B. 1995, in ASP Conf. Ser. 83, Astrophysical Applications of Stellar Pulsations, eds. R. S. Stobie & P. A. Whitelock (San Francisco: ASP), 113
- Chapman, J. M., Sivagnanam, P., Cohen, R. J., & Le Squeren, A. M. 1994, MNRAS, 268, 475
- Cohen, R. J. 1989, RPPh, 52, 881
- Diamond, P. J., Norris, R. P., & Booth, R. S. 1984, MNRAS, 207, 611
- Elitzur, M. 1976, ApJ, 203, 124
- Frail, D. A., Goss, W. M., & Slysh, V. I. 1994, ApJ, 424, L111
- Frank, A., & Mellema, G. 1994, ApJ, 430, 800
- Frater, R. H., Brooks, J. W., & Whiteoak, J. B. 1992, JEEEA, 12, 103
- García-Segura, G., Langer, N., Różyczka, M., & Franco, J. 1999, ApJ, 517, 767
- Gaume, R. A., & Mutel, R. M. 1987, ApJSS, 65, 193
- Gledhill, T. M., Yates, J. A., & Richards, A. M. S. 2001, MNRAS, 328, 301

- Haynes, R. F., & Caswell, J. L. 1977, MNRAS, 178, 219
- Herman, J., & Habing, H. J. 1985, A&AS, 59, 523
- Kwok, S., Purton, C. R., & Fitzgerald, P. M. 1978, ApJ, 219, L125
- Lockett, P., Gauthier, E., & Elitzur, M. 1999, ApJ, 511, 235
- Manchado, A., Villaver, E., Stanghellini, L., & Guerrero, M. A. 2000, in ASP Conf. Ser. 199, Asymmetrical Planetary Nebulae II: From Origins to Microstructures, eds. J. H. Kastner, N. Soker, & S. Rappaport (San Francisco: ASP), 17
- Reid, M. J., & Muhleman, D. O. 1978, ApJ, 220, 229
- Sahai, R., & Trauger, J. T. 1998, AJ, 116, 1357
- Sault, R. J., Teuben, P. J., & Wright, M. C. H. 1995, in ASP Conf. Ser. 77, Astronomical Data Analysis Software and Systems IV, eds. R. A. Shaw, H. E. Payne, & J. J. E. Hayes (San Francisco: ASP), 433
- Sevenster, M. N., Chapman, J. M., Habing, H. J., Killeen, N. E. B., & Lindqvist, M. 1997a, A&AS, 122, 79
- Sevenster, M. N., Chapman, J. M., Habing, H. J., Killeen, N. E. B., & Lindqvist, M. 1997b, A&AS, 124, 509
- Sevenster, M. N., & Chapman, J. M. 2001, ApJ, 546, L119
- Sevenster, M. N., van Langevelde, H. J., Moody, R. A., Chapman, J. M., Habing, H. J., & Killeen, N. E. B. 2001, A&A, 366, 481
- Sevenster, M. N. 2002a, AJ, 123, 2772
- Sevenster, M. N. 2002b, AJ, 123, 2788
- Sivagnanam, P., & David, P. 1999, MNRAS, 304, 622
- Soker, N. 2001, ApJ, 558, 157
- Staveley-Smith, L. 1985, PhD thesis, University of Manchester
- Su, K. Y. L., Hrivnak, B. J., & Kwok, S. 2001, AJ, 122, 1525
- Ueta, T., Meixner, M., & Bobrowsky, M. 2000, ApJ, 528, 861

- van der Veen, W. E. C. J. 1989, *A&A*, 210, 127
- van der Veen, W. E. C. J., & Habing, H. J. 1988, *A&A*, 194, 125
- van Hoof, P. A. M., Oudmaijer, R. D., & Waters, L. B. F. M. 1997, *MNRAS*, 289, 371
- van Langevelde, H. J., van der Heiden, R., & Schooneveld, C. 1990, *A&A*, 239, 193
- Wardle, M. 1999, *ApJ*, 525, L101
- Welty, A. D., Fix, J. D., & Mutel, R. L. 1987, *ApJ*, 318, 852
- Wood, P. R. 2000, in *ASP Conf. Ser. 199, Asymmetrical Planetary Nebulae II: From Origins to Microstructures*, eds. J. H. Kastner, N. Soker, & S. Rappaport (San Francisco: ASP), 51
- Zijlstra, A. A., Chapman, J. M., te Lintel Hekkert, P., Likkell, L., Comeron, F., Norris, R. P., Molster, F. J., & Cohen, R. J. 2001, *MNRAS*, 322, 280

Table 1. Source data.

| Identifier | Iras Name | RA (J2000) | Dec (J2000) | V_{lsr} (km/s) | IRAS Fluxes | | | MSX Fluxes | | | | Classification | |
|------------|--------------|---------------|----------------|---------------------|------------------|------------------|------------------|---------------|------------------|------------------|------------------|----------------|--------|
| | | | | | S_{12} (Jy) | S_{25} (Jy) | S_{60} (Jy) | S_8 (Jy) | S_{12} (Jy) | S_{15} (Jy) | S_{21} (Jy) | (MSX) | (IRAS) |
| d3 | 14341 – 6211 | 14:38:04.961 | –62:24:46.83 | –22.7 | 2.82 | 13.21 | 5.68 | 0.84 | 2.96 | 5.22 | 11.42 | Quad I | RI |
| d29 | 15254 – 5621 | 15:29:19.347 | –56:31:22.33 | –70.8 | 84.08 | 522.40 | 3011.00 | 35.01 | 105.70 | 157.74 | 424.89 | Quad I | RI |
| d34 | 15338 – 5202 | 15:37:31.772 | –52:12:13.15 | –144.6 | ... | ... | ... | 0.80 | 2.02 | 3.41 | 10.90 | Quad I | ... |
| d39 | 15367 – 5420 | 15:40:38.278 | –54:30:18.59 | –102.3 | 1.85 | 6.05 | 13.39 | ... | ... | ... | ... | ... | LI |
| d46 | 15445 – 5449 | 15:48:19.498 | –54:58:21.52 | –140.2 | ... | ... | ... | 0.57 | 5.08 | 13.65 | 52.81 | Quad I | ... |
| d47 | 15452 – 5459 | 15:49:11.398 | –55:08:51.77 | –57.8 | 87.05 | 242.70 | 273.60 | ... | ... | ... | ... | ... | LI |
| d56 | 15514 – 5323 | 15:55:20.690 | –53:32:45.07 | –59.8 | 32.06 | 87.93 | 126.20 | 26.61 | 41.05 | 72.38 | 74.20 | ... | LI |
| d62 | 15544 – 5332 | 15:58:18.830 | –53:40:40.20 | –118.3 | 4.64 | 15.54 | 41.55 | 2.85 | 4.29 | 6.42 | 8.59 | ... | LI |
| d93 | 16209 – 4714 | 16:24:33.912 | –47:21:29.56 | –82.6 | 1.17 | 18.87 | 20.68 | ... | ... | ... | ... | ... | RI |
| d103 | 16314 – 5018 | 16:35:14.944 | –50:24:15.19 | –51.9 | 27.74 | 20.91 | 2.33 | 4.91 | 12.82 | 10.10 | 12.92 | Quad IV | ... |
| d117 | 16372 – 4808 | 16:40:55.829 | –48:13:58.34 | –90.6 | ... | ... | ... | 0.77 | 1.99 | 3.66 | 11.10 | Quad I | ... |
| d150 | 16507 – 4810 | 16:54:30.953 | –48:15:21.24 | –96.4 | 1.08 | 12.56 | 8.96 | ... | ... | ... | ... | ... | RI |
| d168 | 17004 – 4119 | 17:03:56.206 | –41:23:59.25 | –4.5 | 128.10 | 322.60 | 373.10 | 118.24 | 146.74 | 254.77 | 322.18 | ... | LI |
| d189 | 17088 – 4221 | 17:12:22.806 | –42:25:09.82 | 2.8 | 42.70 | 128.30 | 106.80 | 11.91 | 44.88 | 89.24 | 110.41 | Quad IV | ... |
| b5 | 17097 – 3624 | 17:13:04.994 | –36:27:54.34 | –33.0 | 1.52 | 6.61 | 10.11 | ... | ... | ... | ... | ... | RI |
| d190 | 17103 – 3702 | 17:13:44.339 | –37:06:10.95 | –41.0 | 32.08 | 335.90 | 849.70 | ... | ... | ... | ... | ... | RI |
| b11 | 17150 – 3224 | 17:18:19.889 | –32:27:21.96 | 25.3 | 57.92 | 322.30 | 268.30 | 13.07 | 62.04 | 130.90 | 296.48 | Quad I | RI |
| d197 | 17151 – 3845 | 17:18:34.776 | –38:48:57.37 | –178.2 | ... | ... | ... | 0.23 | 1.25 | 3.05 | 6.27 | Quad I | ... |
| b14 | 17164 – 3226 | 17:19:40.776 | –32:29:51.69 | 87.4 | 0.96 | 9.45 | 17.74 | 0.19 | 1.79 | 2.25 | 6.33 | Quad I | RI |
| b15 | 17162 – 3751 | 17:19:42.067 | –37:54:55.16 | –79.0 | ... | ... | ... | 0.51 | 1.56 | 1.88 | 3.82 | Quad I | ... |
| b17 | 17168 – 3736 | 17:20:15.047 | –37:39:34.31 | –6.0 | 9.78 | 36.98 | 47.89 | 1.72 | 10.06 | 23.32 | 28.77 | Quad IV | RI |
| d200 | 17188 – 3838 | 17:22:18.780 | –38:41:40.13 | –92.1 | 9.31 | 15.92 | 21.70 | ... | ... | ... | ... | ... | LI |
| b25 | 17193 – 3546 | 17:22:42.634 | –35:49:31.60 | 17.4 | 3.09 | 6.38 | 33.58 | 0.87 | 1.84 | 3.14 | 3.10 | ... | LI |
| b30 | 17205 – 3556 | 17:23:57.403 | –35:58:50.31 | 70.7 | 2.36 | 3.21 | 17.44 | 3.36 | 5.15 | 5.87 | 5.68 | ... | LI |
| b31 | 17207 – 3632 | 17:24:07.277 | –36:35:40.45 | –143.9 | 6.23 | 14.94 | 22.68 | ... | ... | ... | ... | ... | LI |
| b33 | 17227 – 3623 | 17:26:07.344 | –36:26:15.08 | –24.2 | ... | ... | ... | 0.20 | 1.51 | 2.00 | 2.89 | Quad IV | ... |
| b34 | 17230 – 3348 | 17:26:18.783 | –33:51:20.81 | –208.2 | 2.60 | 7.38 | 24.55 | 0.61 | 2.31 | 4.36 | 5.61 | Quad IV | LI |
| d202 | 17245 – 3951 | 17:28:04.637 | –39:53:44.20 | –97.9 | 3.36 | 44.73 | 38.23 | 0.66 | 2.94 | 8.52 | 36.61 | Quad I | RI |
| b44 | 17256 – 3258 | 17:28:55.751 | –33:00:41.86 | –2.3 | 1.76 | 4.30 | 9.66 | 0.58 | –1.35 | 1.89 | –2.60 | ... | LI |
| b62 | 17293 – 3302 | 17:32:39.109 | –33:04:15.89 | 18.9 | 4.12 | 17.80 | 73.83 | ... | ... | ... | ... | ... | RI |
| b68 | 17310 – 3432 | 17:34:20.788 | –34:34:55.41 | –286.3 | 0.84 | 10.85 | 10.87 | ... | ... | ... | ... | ... | RI |
| b70 | 17317 – 2743 | 17:34:53.287 | –27:45:11.18 | 47.4 | 1.04 | 27.65 | 29.54 | ... | ... | ... | ... | ... | RI |
| b96 | 17359 – 2902 | 17:39:07.703 | –29:04:02.60 | –136.6 | 2.04 | 12.38 | 7.61 | 0.43 | 1.67 | 3.13 | 10.24 | Quad I | RI |

Table 1—Continued

| Identifier | Iras Name | RA (J2000) | Dec (J2000) | V_{lsr} (km/s) | IRAS Fluxes | | | MSX Fluxes | | | | Classification | |
|------------|--------------|---------------|----------------|---------------------|------------------|------------------|------------------|---------------|------------------|------------------|------------------|----------------|--------|
| | | | | | S_{12} (Jy) | S_{25} (Jy) | S_{60} (Jy) | S_8 (Jy) | S_{12} (Jy) | S_{15} (Jy) | S_{21} (Jy) | (MSX) | (IRAS) |
| b106 | 17367 – 3134 | 17:39:57.498 | −31:35:57.28 | 70.7 | ... | ... | ... | 0.23 | 1.74 | 1.29 | 3.60 | Quad I | ... |
| b112 | 17370 – 3357 | 17:40:20.199 | −33:59:13.43 | 25.0 | 0.78 | 7.48 | 9.32 | ... | ... | ... | ... | ... | RI |
| b114 | 17371 – 2747 | 17:40:23.069 | −27:49:11.42 | 115.2 | 2.14 | 10.56 | 14.47 | ... | ... | ... | ... | ... | RI |
| b128 | 17385 – 3332 | 17:41:52.278 | −33:33:40.30 | −234.9 | 2.88 | 13.25 | 10.01 | ... | ... | ... | ... | ... | RI |
| b130 | 17390 – 2809 | 17:42:15.569 | −28:10:36.37 | 0.6 | ... | ... | ... | 0.50 | 2.05 | 3.42 | 4.88 | Quad IV | ... |
| b133 | 17392 – 3020 | 17:42:30.517 | −30:22:07.96 | −3.8 | 6.32 | 17.26 | 36.37 | ... | ... | ... | ... | ... | LI |
| b134 | 17393 – 2727 | 17:42:33.161 | −27:28:24.62 | −108.2 | 1.83 | 17.83 | 36.85 | ... | ... | ... | ... | ... | RI |
| b143 | 17404 – 2713 | 17:43:38.042 | −27:14:44.30 | 43.7 | 3.99 | 20.74 | 15.49 | ... | ... | ... | ... | ... | RI |
| b155 | 17414 – 3108 | 17:44:39.771 | −31:10:05.40 | 46.6 | 2.74 | 6.51 | 10.67 | 1.20 | 1.75 | 3.47 | 4.21 | ... | LI |
| b165 | 17426 – 2804 | 17:45:46.658 | −28:05:28.46 | −26.4 | 5.30 | 10.09 | 40.07 | 3.04 | 3.62 | 4.87 | 3.59 | ... | LI |
| b199 | 17461 – 2741 | 17:49:20.912 | −27:41:54.11 | −127.9 | ... | ... | ... | 0.45 | 1.97 | 3.91 | 5.67 | Quad IV | ... |
| b209 | 17479 – 3032 | 17:51:12.148 | −30:33:39.79 | −15.9 | 2.62 | 13.02 | 16.51 | ... | ... | ... | ... | ... | RI |
| b210 | 17482 – 2501 | 17:51:22.846 | −25:01:52.72 | 72.9 | 1.34 | 5.18 | 11.53 | ... | ... | ... | ... | ... | RI |
| b228 | 17506 – 2955 | 17:53:50.715 | −29:55:28.29 | 182.0 | 1.62 | 6.29 | 6.61 | ... | ... | ... | ... | ... | RI |
| b246 | 17543 – 3102 | 17:57:33.587 | −31:03:02.08 | 121.4 | 2.76 | 21.87 | 24.44 | ... | ... | ... | ... | ... | RI |
| b250 | 17548 – 2753 | 17:57:58.251 | −27:53:19.89 | −185.2 | 1.27 | 16.95 | 21.95 | ... | ... | ... | ... | ... | RI |
| b251 | 17550 – 2120 | 17:58:04.953 | −21:21:07.07 | −21.5 | 5.38 | 21.08 | 30.81 | 1.20 | 4.84 | 11.41 | 16.85 | Quad IV | RI |
| b258 | 17560 – 2027 | 17:59:05.007 | −20:27:23.95 | 204.3 | 1.59 | 15.32 | 17.79 | ... | ... | ... | ... | ... | RI |
| b262 | 17574 – 2403 | 18:00:30.391 | −24:04:01.29 | −7.9 | ... | ... | ... | 26.99 | 153.50 | 318.37 | 162.80 | Quad I | ... |
| b263 | 17576 – 2653 | 18:00:49.500 | −26:53:12.52 | 138.9 | 2.82 | 16.15 | 5.75 | 0.97 | 2.39 | 4.53 | 13.87 | Quad I | RI |
| b266 | 17582 – 2619 | 18:01:21.546 | −26:19:36.75 | 174.7 | 1.38 | 9.28 | 7.92 | 0.34 | 1.80 | 3.31 | 7.42 | Quad I | RI |
| b292 | 18043 – 2116 | 18:07:20.861 | −21:16:10.86 | 87.3 | ... | ... | ... | 0.43 | 1.98 | 4.63 | 5.07 | Quad IV | ... |
| b300 | 18051 – 2415 | 18:08:12.819 | −24:14:36.73 | 120.3 | 1.88 | 8.14 | 9.49 | 0.27 | 1.76 | 3.93 | 5.77 | Quad IV | RI |
| b301 | 18052 – 2016 | 18:08:16.376 | −20:16:11.51 | 51.7 | 21.42 | 32.45 | 82.36 | 16.49 | 28.39 | 29.92 | 27.16 | ... | LI |
| b304 | 18070 – 2332 | 18:10:04.804 | −23:32:09.83 | −63.5 | ... | ... | ... | 1.25 | 4.03 | 8.38 | 10.53 | Quad IV | ... |
| v41 | 18076 – 1853 | 18:10:38.665 | −18:52:58.08 | 42.0 | ... | ... | ... | 1.35 | 10.80 | 33.05 | 141.82 | Quad I | ... |
| v45 | 18087 – 1440 | 18:11:34.086 | −14:39:54.25 | 12.4 | 2.58 | 21.86 | 32.31 | 0.32 | 1.61 | 5.55 | 15.83 | Quad I | RI |
| v50 | 18092 – 2347 | 18:12:20.411 | −23:46:56.95 | 48.8 | 10.95 | 25.81 | 22.44 | ... | ... | ... | ... | ... | LI |
| v53 | 18100 – 1915 | 18:13:03.099 | −19:14:18.66 | 18.1 | 8.70 | 18.25 | 20.12 | ... | ... | ... | ... | ... | LI |
| v56 | 18103 – 1738 | 18:13:20.240 | −17:37:17.35 | 17.0 | 5.34 | 7.16 | 17.01 | 3.10 | 4.04 | 5.19 | 5.02 | ... | LI |
| v67 | 18135 – 1456 | 18:16:25.688 | −14:55:17.16 | −1.1 | 31.02 | 124.40 | 157.60 | 4.95 | 27.13 | 61.13 | 96.13 | Quad IV | RI |
| v87 | 18182 – 1504 | 18:21:06.939 | −15:03:22.11 | 21.5 | 75.13 | 194.30 | 237.00 | ... | ... | ... | ... | ... | LI |
| v117 | 18246 – 1032 | 18:27:23.764 | −10:30:21.71 | 54.5 | 2.18 | 20.25 | 50.37 | 0.96 | 1.87 | 6.17 | 13.73 | ... | RI |

Table 1—Continued

| Identifier | Iras Name | RA (J2000) | Dec (J2000) | V_{lsr} (km/s) | IRAS Fluxes | | | MSX Fluxes | | | | Classification | |
|------------|--------------|---------------|----------------|---------------------|------------------|------------------|------------------|---------------|------------------|------------------|------------------|----------------|--------|
| | | | | | S_{12} (Jy) | S_{25} (Jy) | S_{60} (Jy) | S_8 (Jy) | S_{12} (Jy) | S_{15} (Jy) | S_{21} (Jy) | (MSX) | (IRAS) |
| v120 | 18257 − 1052 | 18:28:30.818 | −10:50:52.99 | 136.2 | 12.38 | 37.68 | 61.23 | 11.54 | 15.62 | 33.54 | 38.40 | ... | LI |
| v121 | 18257 − 1000 | 18:28:30.937 | −09:58:14.33 | 115.8 | 46.32 | 120.50 | 115.90 | 9.75 | 10.65 | 21.33 | 25.19 | ... | LI |
| v132 | 18276 − 1431 | 18:30:30.676 | −14:28:57.78 | 61.2 | 22.65 | 132.00 | 120.00 | 4.76 | 20.85 | 45.39 | 106.73 | Quad I | RI |
| v146 | 18310 − 0806 | 18:33:49.578 | −08:04:01.38 | 106.7 | ... | ... | ... | 0.31 | 1.89 | 4.17 | 11.67 | Quad I | ... |
| v149 | 18314 − 0900 | 18:34:11.303 | −08:58:02.55 | 35.0 | 22.92 | 35.36 | 119.60 | 10.32 | 14.70 | 18.39 | 19.18 | ... | LI |
| v154 | 18327 − 0715 | 18:35:29.202 | −07:13:11.01 | 42.0 | 44.41 | 81.27 | 95.03 | 22.60 | 33.24 | 43.10 | 44.95 | ... | LI |
| v162 | 18342 − 0655 | 18:36:57.999 | −06:53:25.07 | 87.3 | ... | ... | ... | 2.14 | 4.94 | 5.55 | 11.90 | Quad I | ... |
| v169 | 18355 − 0712 | 18:38:15.423 | −07:09:54.16 | 142.9 | 1.73 | 14.34 | 31.14 | ... | ... | ... | ... | ... | RI |
| v172 | 18361 − 0647 | 18:38:50.529 | −06:44:49.85 | 36.3 | 14.79 | 34.16 | 88.73 | 4.12 | 5.98 | 8.30 | 9.01 | ... | LI |
| v189 | 18389 − 0601 | 18:41:35.902 | −05:58:51.02 | 90.8 | 3.52 | 10.37 | 64.61 | 11.11 | 12.49 | 16.75 | 25.44 | ... | LI |
| v204 | 18420 − 0512 | 18:44:41.660 | −05:09:17.00 | 105.6 | 1.03 | 26.72 | 26.22 | 0.26 | 1.49 | 3.01 | 21.74 | Quad I | RI |
| v211 | 18432 − 0149 | 18:45:52.377 | −01:46:42.78 | 66.9 | 25.06 | 52.32 | 48.09 | 12.83 | 19.81 | 30.09 | 33.82 | ... | LI |
| v212 | 18434 − 0202 | 18:46:05.779 | −01:59:17.62 | 37.5 | 13.93 | 19.75 | 61.53 | 7.21 | 9.91 | 12.21 | 10.71 | ... | LI |
| v223 | 18450 − 0148 | 18:47:41.130 | −01:45:11.76 | 33.9 | ... | ... | ... | 2.33 | 23.90 | 55.87 | 88.56 | Quad IV | ... |
| v228 | 18460 − 0254 | 18:48:41.947 | −02:50:29.23 | 98.6 | 111.10 | 279.90 | 237.00 | 100.32 | 140.24 | 227.94 | 276.72 | ... | LI |
| v231 | 18467 − 0238 | 18:49:19.446 | −02:34:49.90 | 68.1 | 5.55 | 37.55 | 57.46 | 1.20 | 5.81 | 12.63 | 23.93 | Quad IV | RI |
| v237 | 18485 + 0642 | 18:50:59.501 | +06:45:57.49 | 95.3 | 3.58 | 21.86 | 25.32 | 0.98 | 3.11 | 7.73 | 16.88 | Quad I | RI |
| v239 | 18488 − 0107 | 18:51:26.252 | −01:03:52.23 | 75.9 | 16.45 | 42.98 | 44.03 | 21.72 | 32.01 | 49.24 | 58.86 | ... | LI |
| v268 | 18588 + 0428 | 19:01:20.032 | +04:32:31.25 | 53.2 | 10.77 | 13.05 | 20.11 | 15.84 | 19.45 | 19.25 | 16.09 | ... | LI |
| v270 | 18596 + 0315 | 19:02:06.259 | +03:20:15.47 | 88.3 | 2.60 | 14.17 | 22.57 | 0.40 | 2.51 | 5.95 | 10.54 | Quad IV | RI |
| v274 | 19024 + 0044 | 19:05:02.155 | +00:48:51.19 | 50.0 | 2.86 | 48.83 | 42.53 | 0.67 | 2.40 | 8.44 | 38.04 | Quad I | RI |
| v280 | 19070 + 0859 | 19:10:21.766 | +09:05:01.43 | 18.2 | ... | ... | ... | 24.12 | 123.46 | 226.82 | 518.96 | Quad I | ... |

Table 2. Schedule of Observations

| Frequency (MHz) | UT date | Typical integration time (min) | Typical rms noise (Jy) |
|--------------------|------------------------|-----------------------------------|---------------------------|
| Parkes Telescope | | | |
| 1612 | 2002 Sep 5-7 | 10 | 0.07 |
| 1665/67 | 2002 Sep 7 | 10 | 0.07 |
| 1665/67 | 2002 Sep 7-8 | 10 | 0.12 |
| 1720 | 2003 Jan 30 | 20 | 0.23 |
| 1720 | 2003 Jan 31 - Feb 1 | 15 | 0.06 |
| 1720 | 2003 Feb 1-2 | 10 | 0.07 |
| 1720 | 2003 Feb 3 | 8 | 0.09 |
| 1720 | 2003 Aug 17 | 20 | 0.10 |
| 1612/65/67 | 2003 Aug 18 | 10 | 0.10 |
| ATCA | | | |
| 1665/67 | 2003 Jul 23/24 + Aug 7 | 14 | 0.03 |
| 1720 | 2003 Aug 08 | 14 | 0.04 |

Table 3. Results from 1612, 1665 and 1667 MHz observations.

[illegible]

Table 3—Continued

| Name | V_b (km s ⁻¹) | S_b (Jy) | I_b (Jy km s ⁻¹) | V_r (km s ⁻¹) | S_r (Jy) | I_r (Jy km s ⁻¹) | $\frac{S_b}{S_r}$ | $\frac{I_b}{I_r}$ | Vrange (km s ⁻¹) | Type | Flag |
|------|--------------------------------|---------------|-----------------------------------|--------------------------------|---------------|-----------------------------------|-------------------|-------------------|---------------------------------|------|------|
| b11 | ... | ... | ... | 24.96 | 3.01 | 4.0 | ... | ... | 3 | S | |
| | 14.23 | 1.72 | 16.0 | ... | ... | ... | ... | ... | 24 | I | |
| | 1.41 | 10.19 | 25.5 | 25.83 | 13.11 | 34.8 | 0.78 | 0.7 | 31 | D | |
| d197 | -193.29 | 7.16 | 10.7 | -163.17 | 3.22 | 6.4 | 2.22 | 1.7 | 33 | D | |
| | -194.08 | 0.60 | 0.4 | ... | ... | ... | ... | ... | 4 | S | # |
| | ... | ... | ... | -162.32 | 0.60 | 0.6 | ... | ... | 3 | - | m |
| b14 | 72.67 | 5.79 | 5.9 | 101.54 | 3.93 | 4.7 | 1.47 | 1.2 | 33 | D | |
| | 72.13 | 0.43 | 0.2 | 101.91 | 0.37 | 0.4 | 1.16 | 0.4 | 33 | D | |
| | 71.86 | 1.46 | 0.6 | 101.56 | 2.13 | 2.6 | 0.69 | 0.2 | 33 | D | |
| b15 | -75.10 | 0.63 | 1.5 | ... | ... | ... | ... | ... | 39 | I | |
| | ... | ... | ... | ... | ... | ... | ... | ... | ... | ... | |
| | ... | ... | ... | ... | ... | ... | ... | ... | ... | ... | |
| b17 | -18.33 | 37.18 | 42.1 | 7.27 | 18.57 | 31.1 | 2.00 | 1.4 | 29 | D | |
| | ... | ... | ... | ... | ... | ... | ... | ... | ... | ... | |
| | -19.11 | 1.00 | 0.2 | 7.15 | 5.54 | 8.0 | 0.18 | 0.0 | 30 | D | |
| d200 | -92.13 | 5.37 | 16.8 | -57.20 | 0.62 | 1.9 | 8.60 | 8.9 | 42 | De | |
| | ... | ... | ... | ... | ... | ... | ... | ... | ... | ... | |
| | ... | ... | ... | ... | ... | ... | ... | ... | ... | ... | |
| b25 | 7.89 | 2.85 | 2.2 | 28.04 | 1.60 | 1.5 | 1.78 | 1.5 | 23 | D | |
| | ... | ... | ... | ... | ... | ... | ... | ... | ... | ... | |
| | ... | ... | ... | ... | ... | ... | ... | ... | ... | ... | |
| b30 | 52.02 | 0.31 | 0.4 | 86.80 | 0.26 | 0.7 | 1.19 | 0.7 | 40 | D | V |
| | ... | ... | ... | ... | ... | ... | ... | ... | ... | ... | |
| | ... | ... | ... | ... | ... | ... | ... | ... | ... | ... | |
| b31 | -161.07 | 3.80 | 3.7 | -127.59 | 1.91 | 1.4 | 1.99 | 2.7 | 36 | D | |
| | ... | ... | ... | ... | ... | ... | ... | ... | ... | ... | |
| | ... | ... | ... | -127.42 | 1.24 | 1.7 | ... | ... | 9 | S | |
| b33 | -36.27 | 1.92 | 3.1 | -11.76 | 0.86 | 2.0 | 2.23 | 1.5 | 36 | D | |
| | ... | ... | ... | ... | ... | ... | ... | ... | ... | ... | |
| | ... | ... | ... | ... | ... | ... | ... | ... | ... | ... | |
| b34 | -218.28 | 7.46 | 9.4 | -198.59 | 2.10 | 2.8 | 3.56 | 3.4 | 23 | D | |
| | -219.08 | 0.67 | 0.3 | ... | ... | ... | ... | ... | 3 | - | m |
| | ... | ... | ... | -198.45 | 0.39 | 0.5 | ... | ... | 4 | - | m# |
| d202 | -109.88 | 29.49 | 38.3 | -84.93 | 36.99 | 55.7 | 0.80 | 0.7 | 27 | D | |
| | -105.20 | 1.77 | 10.3 | -86.85 | 2.28 | 9.9 | 0.77 | 1.0 | 25 | D | |
| | -110.90 | 2.10 | 2.1 | -84.48 | 5.34 | 5.3 | 0.39 | 0.4 | 28 | D | |
| b44 | -34.98 | 0.78 | 0.7 | ... | ... | ... | ... | ... | 7 | S | V |
| | ... | ... | ... | ... | ... | ... | ... | ... | ... | ... | |
| | ... | ... | ... | ... | ... | ... | ... | ... | ... | ... | |
| b62 | 20.01 | 1.80 | 5.4 | ... | ... | ... | ... | ... | 14 | I | |
| | 18.62 | 0.80 | 0.4 | ... | ... | ... | ... | ... | 3 | S | |
| | 18.97 | 0.87 | 8.0 | ... | ... | ... | ... | ... | 24 | I | |
| b68 | -298.54 | 1.19 | 2.7 | -274.42 | 4.69 | 4.8 | 0.25 | 0.6 | 27 | D | |
| | ... | ... | ... | ... | ... | ... | ... | ... | ... | ... | |
| | -299.32 | 0.70 | 0.7 | ... | ... | ... | ... | ... | 7 | S | |

Table 3—Continued

[illegible]

Table 3—Continued

| Name | V_b (km s ⁻¹) | S_b (Jy) | I_b (Jy km s ⁻¹) | V_r (km s ⁻¹) | S_r (Jy) | I_r (Jy km s ⁻¹) | $\frac{S_b}{S_r}$ | $\frac{I_b}{I_r}$ | Vrange (km s ⁻¹) | Type | Flag |
|------|--------------------------------|---------------|-----------------------------------|--------------------------------|---------------|-----------------------------------|-------------------|-------------------|---------------------------------|------|------|
| b228 | 170.21 | 0.45 | 1.1 | 192.64 | 2.11 | 3.4 | 0.21 | 0.3 | 27 | D | |
| | ... | ... | ... | ... | ... | ... | ... | ... | ... | ... | |
| | ... | ... | ... | ... | ... | ... | ... | ... | ... | ... | |
| b246 | 122.04 | 2.78 | 15.1 | ... | ... | ... | ... | ... | 42 | I | V |
| | 126.07 | 0.51 | 6.0 | ... | ... | ... | ... | ... | 39 | I | |
| | ... | ... | ... | ... | ... | ... | ... | ... | ... | ... | |
| b250 | -202.45 | 1.31 | 2.0 | -168.88 | 3.32 | 3.4 | 0.39 | 0.6 | 35 | D | |
| | ... | ... | ... | ... | ... | ... | ... | ... | ... | ... | |
| | -202.66 | 0.74 | 0.9 | -168.61 | 1.16 | 2.8 | 0.64 | 0.3 | 39 | D | |
| b251 | -34.55 | 12.91 | 18.7 | -8.13 | 12.36 | 18.4 | 1.04 | 1.0 | 29 | D | |
| | -35.20 | 1.16 | 1.5 | ... | ... | ... | ... | ... | 5 | S | |
| | -35.28 | 1.69 | 2.3 | -7.62 | 3.25 | 5.1 | 0.52 | 0.4 | 30 | D | |
| b258 | 191.06 | 7.22 | 12.4 | 217.58 | 3.83 | 8.0 | 1.88 | 1.5 | 29 | D | |
| | 192.17 | 0.59 | 6.3 | ... | ... | ... | ... | ... | 40 | I | |
| | 190.06 | 0.67 | 0.9 | 219.77 | 0.41 | 0.9 | 1.62 | 1.0 | 33 | D | |
| b262 | -21.31 | 11.58 | 32.4 | ... | ... | ... | ... | ... | 50 | I | |
| | 10.90 | 6.24 | 47.0 | ... | ... | ... | ... | ... | 50 | I | |
| | -29.33 | 18.37 | 218.2 | ... | ... | ... | ... | ... | 62 | I | |
| b263 | 138.30 | 0.69 | 9.1 | ... | ... | ... | ... | ... | 48 | I | |
| | 138.65 | 1.09 | 9.3 | ... | ... | ... | ... | ... | 26 | I | |
| | ... | ... | ... | ... | ... | ... | ... | ... | ... | ... | |
| b266 | 164.10 | 3.58 | 3.1 | 186.81 | 3.71 | 3.1 | 0.97 | 1.0 | 25 | D | |
| | ... | ... | ... | ... | ... | ... | ... | ... | ... | ... | |
| | ... | ... | ... | ... | ... | ... | ... | ... | ... | ... | |
| b292 | 70.40 | 18.85 | 58.8 | 99.28 | 0.35 | 0.9 | 53.84 | 62.0 | 36 | De | |
| | 69.70 | 7.37 | 5.2 | 103.97 | 1.64 | 1.9 | 4.50 | 2.7 | 36 | D | |
| | ... | ... | ... | ... | ... | ... | ... | ... | ... | ... | |
| b300 | 105.60 | 2.48 | 2.2 | 135.48 | 0.80 | 1.4 | 3.12 | 1.6 | 32 | D | |
| | ... | ... | ... | ... | ... | ... | ... | ... | ... | ... | |
| | 106.87 | 0.53 | 0.5 | ... | ... | ... | ... | ... | 8 | S | # |
| b301 | 23.30 | 1.15 | 6.4 | 79.59 | 3.03 | 13.2 | 0.38 | 0.5 | 64 | D | |
| | ... | ... | ... | ... | ... | ... | ... | ... | ... | ... | |
| | ... | ... | ... | ... | ... | ... | ... | ... | ... | ... | |
| b304 | -74.39 | 4.74 | 6.7 | -52.25 | 3.91 | 6.0 | 1.21 | 1.1 | 25 | D | |
| | -74.76 | 0.36 | 0.2 | ... | ... | ... | ... | ... | 2 | - | m# |
| | -75.37 | 0.49 | 0.5 | -51.93 | 0.77 | 0.5 | 0.63 | 0.9 | 25 | D | # |
| v41 | 20.51 | 7.06 | 46.2 | 64.09 | 33.71 | 274.1 | 0.21 | 0.2 | 65 | Dw | |
| | ... | ... | ... | 62.46 | 1.68 | 11.1 | ... | ... | 16 | I | |
| | 13.01 | 0.98 | 9.0 | 65.97 | 2.27 | 13.9 | 0.43 | 0.6 | 75 | I | |
| v45 | -2.37 | 11.28 | 9.1 | 26.77 | 11.54 | 7.4 | 0.98 | 1.2 | 31 | D | |
| | ... | ... | ... | 26.27 | 0.45 | 0.1 | ... | ... | 18 | I | # |
| | -2.81 | 0.78 | 1.4 | 27.14 | 0.71 | 0.8 | 1.11 | 1.7 | 32 | D | |
| v50 | 30.81 | 0.68 | 0.9 | 66.85 | 0.39 | 1.1 | 1.72 | 0.7 | 38 | D | |
| | ... | ... | ... | ... | ... | ... | ... | ... | ... | ... | |
| | 29.03 | 0.38 | 1.3 | 66.99 | 0.38 | 1.3 | 0.99 | 0.9 | 42 | D | |

Table 3—Continued

| Name | V_b (km s ⁻¹) | S_b (Jy) | I_b (Jy km s ⁻¹) | V_r (km s ⁻¹) | S_r (Jy) | I_r (Jy km s ⁻¹) | $\frac{S_b}{S_r}$ | $\frac{I_b}{I_r}$ | Vrange (km s ⁻¹) | Type | Flag |
|------|--------------------------------|---------------|-----------------------------------|--------------------------------|---------------|-----------------------------------|-------------------|-------------------|---------------------------------|------|------|
| v53 | 3.49 | 1.72 | 1.6 | 31.45 | 3.21 | 1.9 | 0.54 | 0.8 | 32 | D | |
| | 4.05 | 0.26 | 1.1 | ... | ... | ... | ... | ... | 10 | - | m |
| | 3.17 | 0.44 | 3.3 | ... | ... | ... | ... | ... | 36 | I | |
| v56 | -3.77 | 1.04 | 1.9 | 39.71 | 0.53 | 1.3 | 1.96 | 1.4 | 48 | D | v |
| | ... | ... | ... | ... | ... | ... | ... | ... | ... | ... | |
| | ... | ... | ... | ... | ... | ... | ... | ... | ... | ... | |
| v67 | -15.26 | 61.79 | 84.7 | 13.06 | 47.87 | 66.5 | 1.29 | 1.3 | 33 | D | v |
| | -9.43 | 0.98 | 5.9 | ... | ... | ... | ... | ... | 32 | I | |
| | -14.52 | 1.33 | 6.4 | 15.25 | 11.44 | 12.9 | 0.12 | 0.5 | 33 | De | |
| v87 | -1.45 | 9.55 | 53.0 | 43.03 | 18.62 | 57.8 | 0.51 | 0.9 | 48 | D | |
| | ... | ... | ... | ... | ... | ... | ... | ... | ... | ... | |
| | -1.78 | 2.10 | 9.2 | 44.69 | 3.41 | 24.0 | 0.62 | 0.4 | 51 | D | |
| v117 | 60.75 | 14.56 | 131.6 | ... | ... | ... | ... | ... | 74 | I | v |
| | 58.37 | 4.31 | 42.0 | ... | ... | ... | ... | ... | 50 | I | |
| | 40.54 | 0.99 | 19.6 | ... | ... | ... | ... | ... | 89 | I | |
| v120 | 118.08 | 13.69 | 24.5 | 154.58 | 6.40 | 22.7 | 2.14 | 1.1 | 39 | D | |
| | ... | ... | ... | ... | ... | ... | ... | ... | ... | ... | |
| | 117.31 | 3.28 | 8.2 | 155.45 | 2.96 | 11.7 | 1.11 | 0.7 | 41 | D | |
| v121 | 97.82 | 22.60 | 67.7 | 134.14 | 24.89 | 40.7 | 0.91 | 1.7 | 41 | D | v |
| | ... | ... | ... | ... | ... | ... | ... | ... | ... | ... | |
| | 96.04 | 3.40 | 7.3 | 132.51 | 0.83 | 7.2 | 4.12 | 1.0 | 46 | D | |
| v132 | 48.71 | 60.29 | 118.6 | 72.95 | 89.96 | 170.7 | 0.67 | 0.7 | 28 | D | # |
| | 47.75 | 5.47 | 3.3 | 72.43 | 1.09 | 3.3 | 5.02 | 1.0 | 29 | D | |
| | 47.66 | 0.86 | 1.6 | 74.36 | 15.69 | 14.5 | 0.05 | 0.1 | 29 | De | |
| v146 | 98.00 | 1.84 | 7.8 | 117.16 | 10.57 | 19.8 | 0.17 | 0.4 | 25 | D | v |
| | ... | ... | ... | ... | ... | ... | ... | ... | ... | ... | |
| | 94.33 | 0.34 | 1.1 | ... | ... | ... | ... | ... | 27 | - | m |
| v149 | 20.38 | 12.02 | 26.3 | 49.25 | 13.71 | 25.8 | 0.88 | 1.0 | 32 | D | |
| | ... | ... | ... | ... | ... | ... | ... | ... | ... | ... | |
| | ... | ... | ... | ... | ... | ... | ... | ... | ... | ... | |
| v154 | 21.41 | 5.93 | 20.8 | 59.54 | 3.24 | 18.1 | 1.83 | 1.1 | 46 | D | v |
| | ... | ... | ... | ... | ... | ... | ... | ... | ... | ... | |
| | ... | ... | ... | ... | ... | ... | ... | ... | ... | ... | |
| v162 | 73.31 | 3.67 | 5.9 | 102.91 | 1.69 | 4.9 | 2.17 | 1.2 | 35 | D | v |
| | ... | ... | ... | ... | ... | ... | ... | ... | ... | ... | |
| | ... | ... | ... | ... | ... | ... | ... | ... | ... | ... | |
| v169 | 130.30 | 8.67 | 11.2 | 155.18 | 6.90 | 10.0 | 1.26 | 1.1 | 27 | D | |
| | ... | ... | ... | ... | ... | ... | ... | ... | ... | ... | |
| | 128.85 | 0.42 | 0.2 | 155.39 | 0.86 | 1.1 | 0.49 | 0.2 | 29 | D | # |
| v172 | 19.98 | 6.41 | 16.1 | 53.75 | 4.63 | 15.5 | 1.39 | 1.0 | 37 | D | v |
| | ... | ... | ... | ... | ... | ... | ... | ... | ... | ... | |
| | ... | ... | ... | ... | ... | ... | ... | ... | ... | ... | |
| v189 | 89.42 | 0.59 | 1.4 | ... | ... | ... | ... | ... | 8 | S | v |
| | ... | ... | ... | ... | ... | ... | ... | ... | ... | ... | |
| | 89.24 | 1.13 | 1.4 | ... | ... | ... | ... | ... | 8 | S | |

Table 3—Continued

| Name | V_b (km s ⁻¹) | S_b (Jy) | I_b (Jy km s ⁻¹) | V_r (km s ⁻¹) | S_r (Jy) | I_r (Jy km s ⁻¹) | $\frac{S_b}{S_r}$ | $\frac{I_b}{I_r}$ | Vrange (km s ⁻¹) | Type | Flag |
|------|--------------------------------|---------------|-----------------------------------|--------------------------------|---------------|-----------------------------------|-------------------|-------------------|---------------------------------|------|------|
| v204 | 93.17 | 7.64 | 17.2 | 118.25 | 5.67 | 19.1 | 1.35 | 0.9 | 29 | D | |
| | ... | ... | ... | ... | ... | ... | ... | ... | ... | ... | |
| | 92.61 | 2.58 | 3.4 | ... | ... | ... | ... | ... | 4 | S | |
| v211 | 48.93 | 8.44 | 15.3 | 84.07 | 5.30 | 11.4 | 1.59 | 1.3 | 37 | D | |
| | ... | ... | ... | ... | ... | ... | ... | ... | ... | ... | |
| | 48.34 | 0.58 | 1.2 | 84.45 | 2.15 | 0.6 | 0.27 | 2.0 | 41 | D | |
| v212 | 18.38 | 1.05 | 4.0 | 56.60 | 5.30 | 7.0 | 0.20 | 0.6 | 44 | D | v |
| | ... | ... | ... | ... | ... | ... | ... | ... | ... | ... | |
| | ... | ... | ... | ... | ... | ... | ... | ... | ... | ... | |
| v223 | 27.73 | 2.71 | 2.1 | 40.35 | 38.59 | 33.5 | 0.07 | 0.1 | 17 | De | v |
| | 27.69 | 3.39 | 4.2 | 40.51 | 2.91 | 5.4 | 1.16 | 0.8 | 16 | D | |
| | 27.95 | 3.00 | 7.4 | 40.69 | 3.99 | 2.9 | 0.75 | 2.5 | 21 | D | |
| v228 | 78.52 | 74.78 | 216.0 | 119.29 | 90.35 | 279.1 | 0.83 | 0.8 | 44 | D | v |
| | ... | ... | ... | ... | ... | ... | ... | ... | ... | ... | |
| | 77.35 | 3.50 | 8.7 | 120.49 | 10.04 | 25.1 | 0.35 | 0.3 | 46 | D | |
| v231 | 60.19 | 9.79 | 56.2 | ... | ... | ... | ... | ... | 71 | I | |
| | 59.87 | 5.55 | 75.9 | ... | ... | ... | ... | ... | 64 | I | |
| | 55.39 | 1.47 | 39.1 | ... | ... | ... | ... | ... | 78 | I | |
| v237 | 82.18 | 16.50 | 11.8 | 108.42 | 36.46 | 28.1 | 0.45 | 0.4 | 28 | D | |
| | ... | ... | ... | 109.07 | 1.08 | 4.5 | ... | ... | 50 | I | |
| | 81.39 | 1.21 | 0.7 | 109.24 | 1.76 | 1.3 | 0.69 | 0.6 | 30 | D | |
| v239 | 55.20 | 7.62 | 26.0 | 95.87 | 4.52 | 13.3 | 1.69 | 2.0 | 44 | D | v |
| | ... | ... | ... | ... | ... | ... | ... | ... | ... | ... | |
| | ... | ... | ... | 96.62 | 1.67 | 4.5 | ... | ... | 12 | S | # |
| v268 | 29.44 | 0.79 | 2.7 | 74.11 | 0.57 | 1.8 | 1.39 | 1.5 | 51 | D | |
| | ... | ... | ... | ... | ... | ... | ... | ... | ... | ... | |
| | ... | ... | ... | ... | ... | ... | ... | ... | ... | ... | |
| v270 | 76.77 | 8.98 | 24.2 | 101.92 | 8.47 | 20.7 | 1.06 | 1.2 | 31 | D | |
| | ... | ... | ... | 101.48 | 0.33 | 0.6 | ... | ... | 34 | - | m |
| | 74.77 | 0.45 | 0.7 | 103.59 | 0.71 | 0.8 | 0.63 | 0.9 | 32 | D | |
| v274 | 40.65 | 4.61 | 35.4 | 62.81 | 4.84 | 31.6 | 0.95 | 1.1 | 50 | Dw | |
| | 40.42 | 1.95 | 4.7 | 61.32 | 1.54 | 8.3 | 1.27 | 0.6 | 33 | Dw | |
| | 32.33 | 0.42 | 4.8 | 76.00 | 0.28 | 2.4 | 1.51 | 2.0 | 68 | Dw | |

^VSources which are more than 30% variable at 1612 MHz

^{2nd}d47 has two lines for 1612 MHz data

^mMarginal detection, Sept 2002 data

[#]August 2003 data

^{m#}Marginal detection, August 2003 data

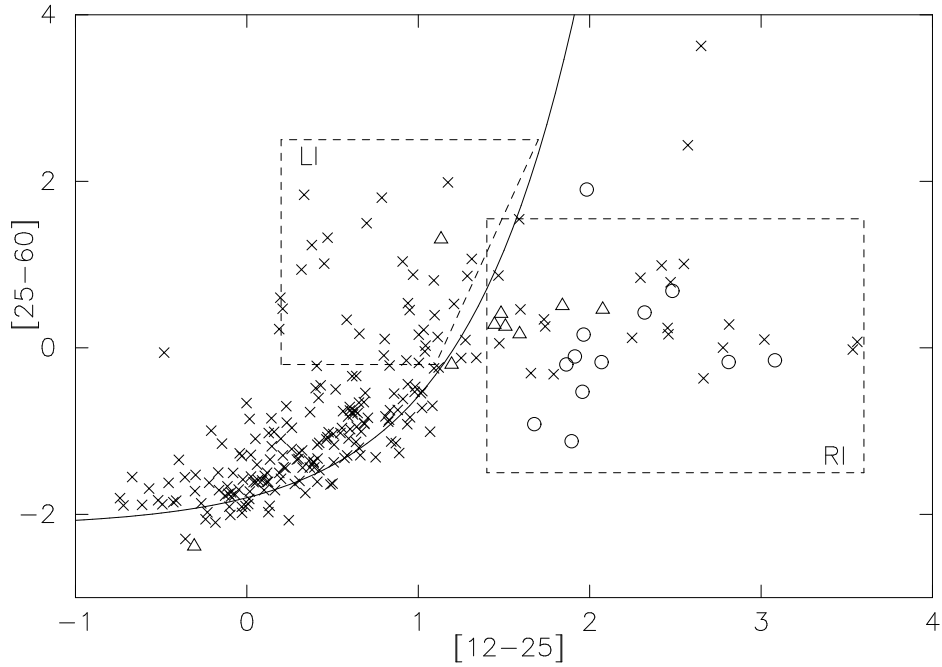


Fig. 1.— An IRAS two-colour diagram for sources in the ATCA/VLA survey. The solid line is the evolutionary sequence for AGB stars defined by van der Veen & Habing (1988). The regions marked ‘RI’ and ‘LI’ are associated with post-AGB stars (Sevenster 2002a,b). The three sources above the RI box are identified as star-formation regions. The crosses show sources with IRAS colours only. Triangles show sources with MSX colours that correspond to Quad IV (early post-AGB stars) of Figure 2. Circles show sources with MSX colours that correspond to Quad I (late post-AGB stars) of Figure 2.

Table 4. Number of detections by frequency and spectral profile.

| Profile class | 1612 MHz | 1665 MHz | 1667 MHz |
|---------------|-----------|-----------|-----------|
| D | 60 | 5 | 23 |
| DD | 1 | 0 | 0 |
| De | 4 | 0 | 2 |
| Dw | 4 | 1 | 1 |
| I | 13 | 16 | 10 |
| S | 4 | 5 | 9 |
| | 86 | 27 | 45 |

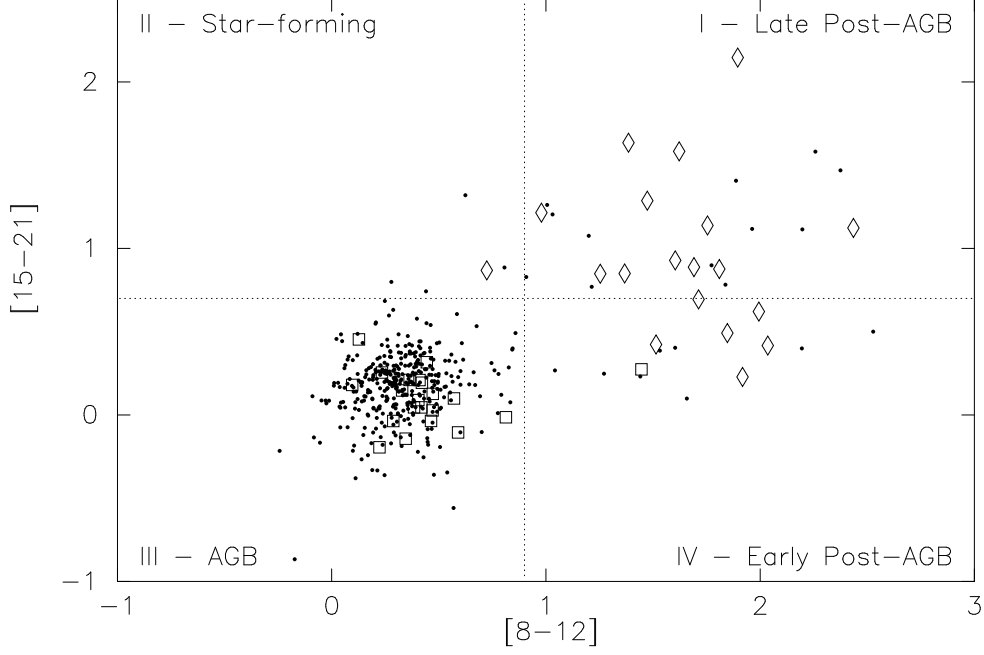


Fig. 2.— An MSX two-colour diagram for sources in the ATCA/VLA survey. Following Sevenster (2002a), this is divided into four quadrants according to minima which are seen in bimodal distributions of the MSX infrared colours $[8-12]$ and $[15-21]$. The four quadrants I-IV are thought to contain in turn late post-AGB stars, star-formation regions, AGB stars and early post-AGB stars. The dots show sources with MSX colours only. Squares show sources with IRAS colours in the LI region of Figure 1. Diamonds show sources with IRAS colours in the RI region of Figure 1.

Table 5. The number of objects from each source group with emission at each of 1612, 1665 and 1667 MHz.

| | RI | LI | Quad I | Quad IV |
|----------|----|----|--------|---------|
| 1612 MHz | 38 | 30 | 22 | 15 |
| 1665 MHz | 19 | 1 | 12 | 6 |
| 1667 MHz | 24 | 14 | 11 | 10 |

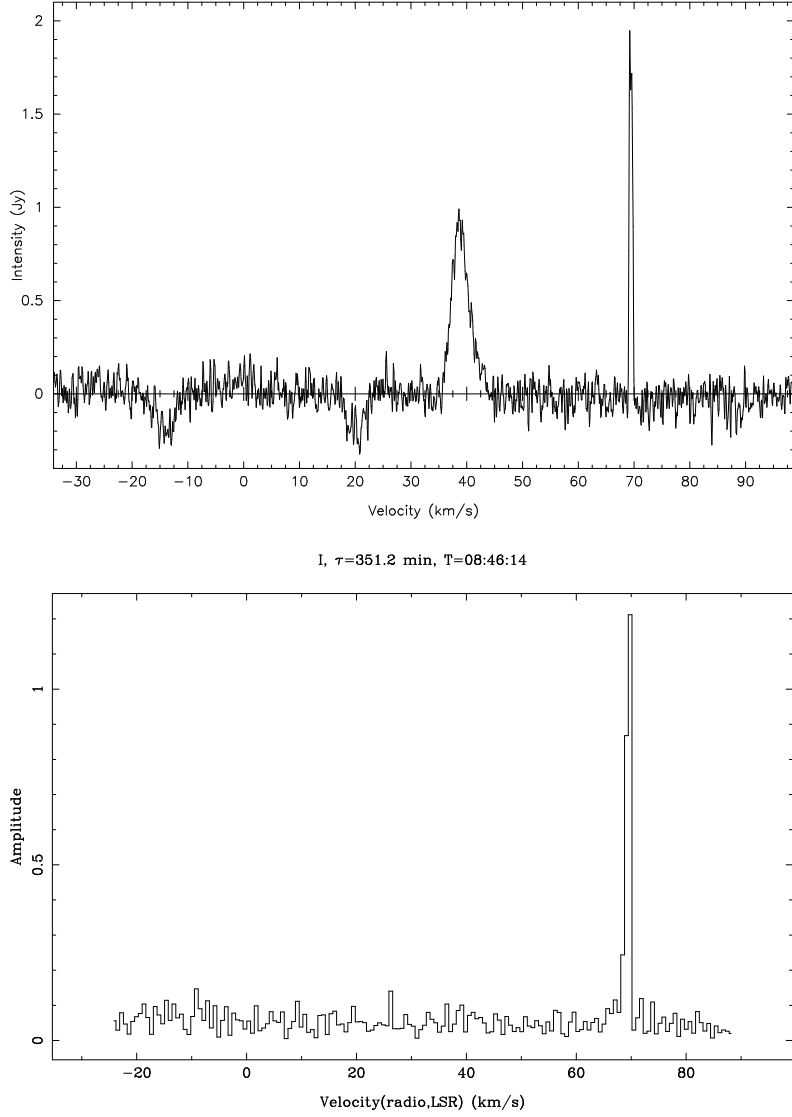


Fig. 3.— Total intensity 1720 MHz spectra for b292. The top spectrum is from an observation at Parkes on 2003 February 2. The velocity resolution is 0.18 km s^{-1} . The bottom spectrum was obtained with the ATCA on 2003 August 8 with a velocity resolution of 0.88 km s^{-1} . The broad emission and absorption features in the Parkes spectrum are absent from the ATCA spectrum, showing that these emission and absorption features are spatially extended and are not associated with the compact stellar source. The smaller peak flux density at 69.2 km s^{-1} in the ATCA spectrum is due to the dilution effect caused by the broader velocity resolution of the ATCA spectrum.

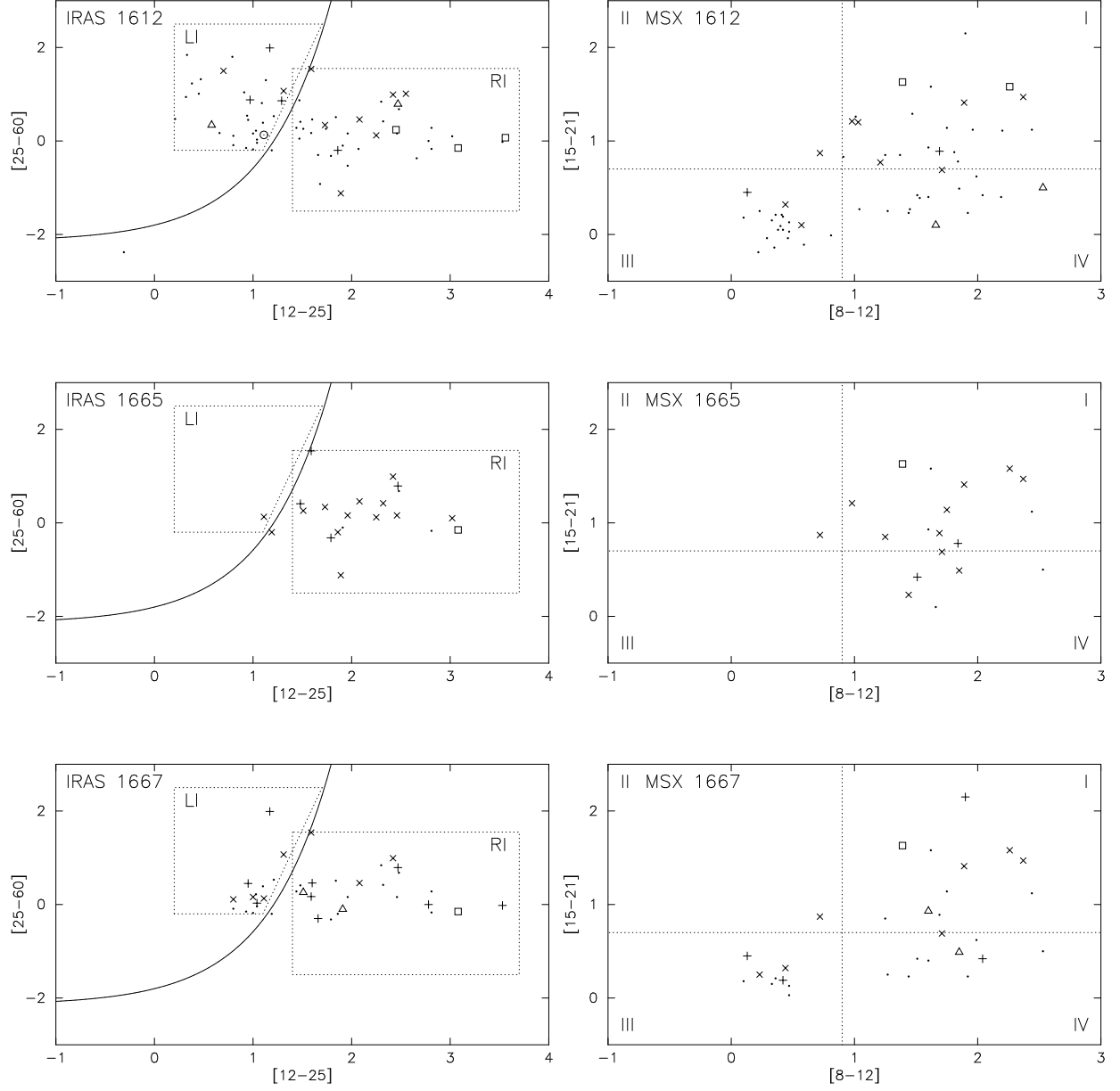


Fig. 4.— IRAS (left) and MSX (right) two-colour diagrams with sources with 1612, 1665 and 1667 MHz spectra plotted. Symbols are according to spectral profile classification: D · Dw □ De △ DD ⊙ I × and S + .

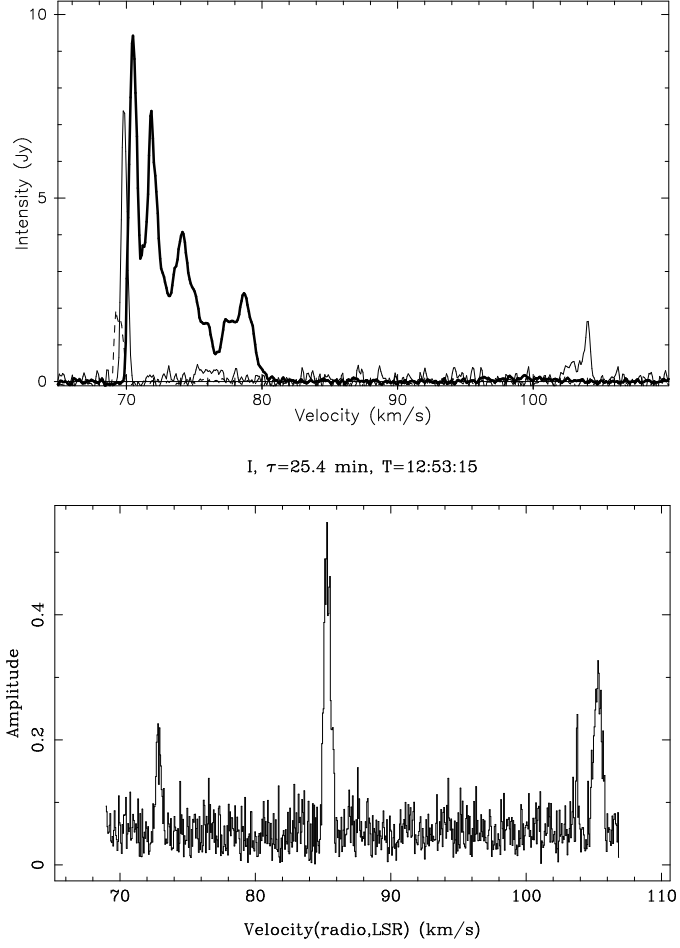


Fig. 5.— (top) Overlay of Parkes 1612 (bold), 1665 (thin) and 1720 MHz (dashed) spectra for b292. The 1612 MHz spectrum is scaled by 0.5. (bottom) ATCA water maser spectrum of b292. These spectra show the complex velocity structure of the different maser types around b292.

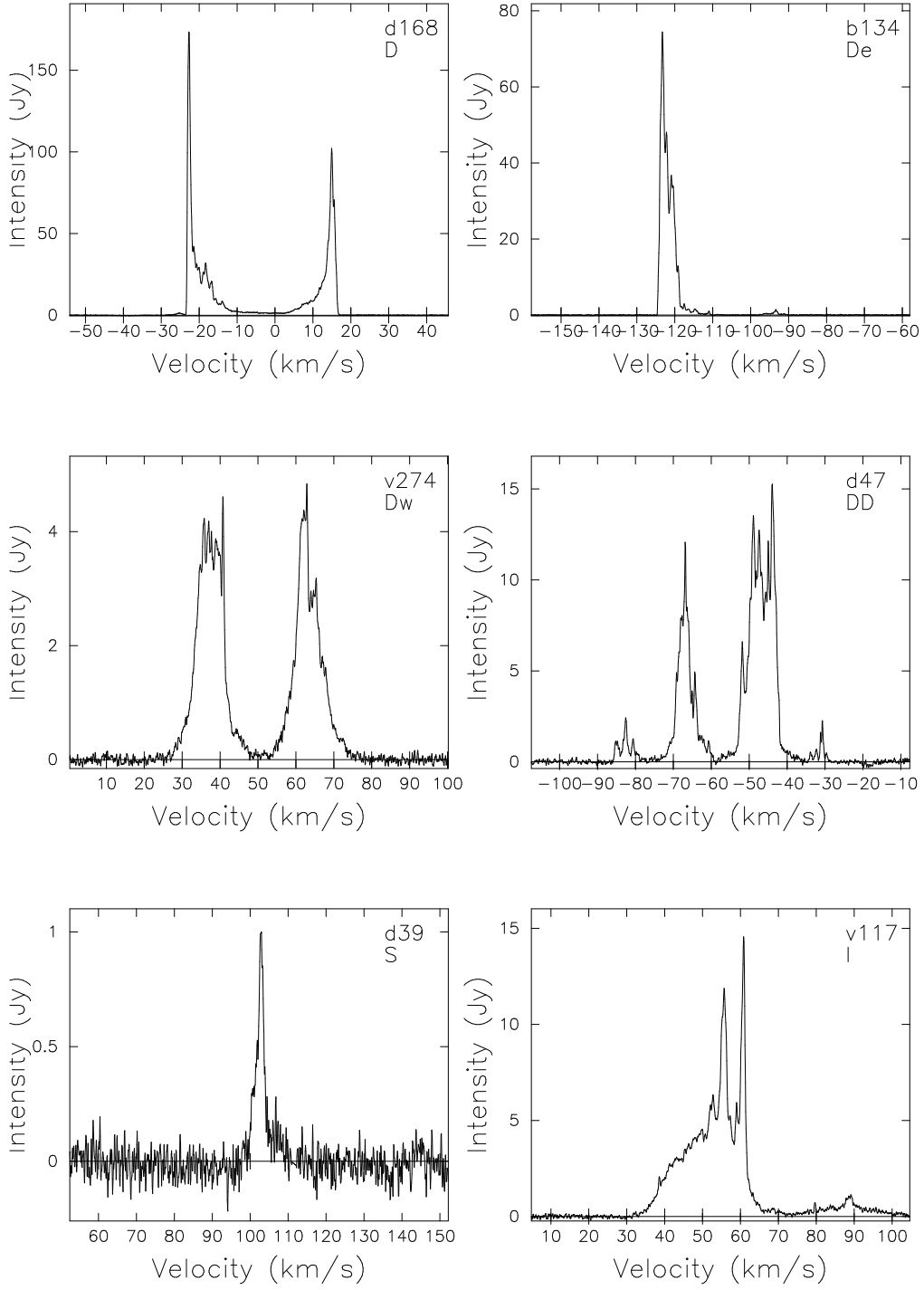
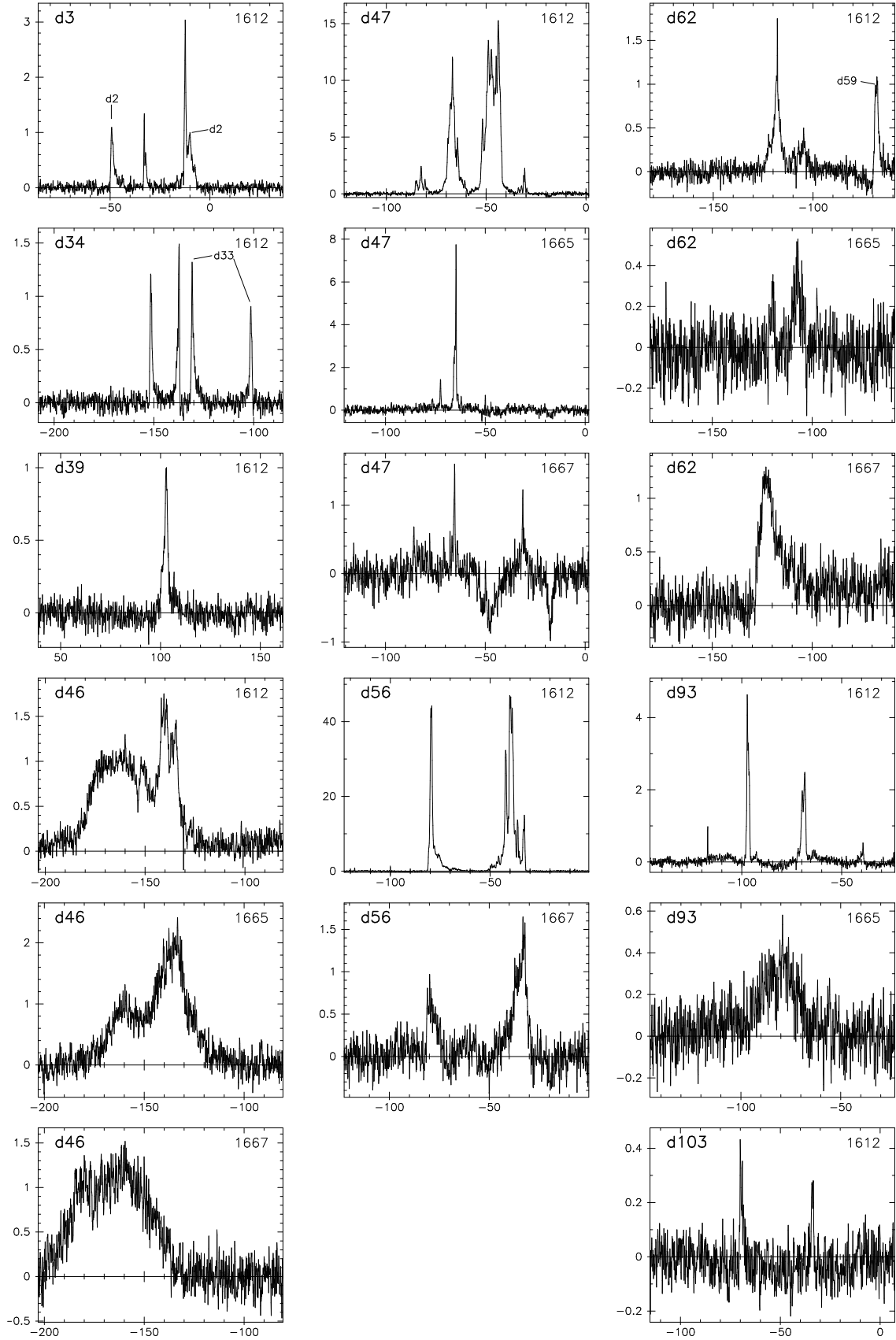
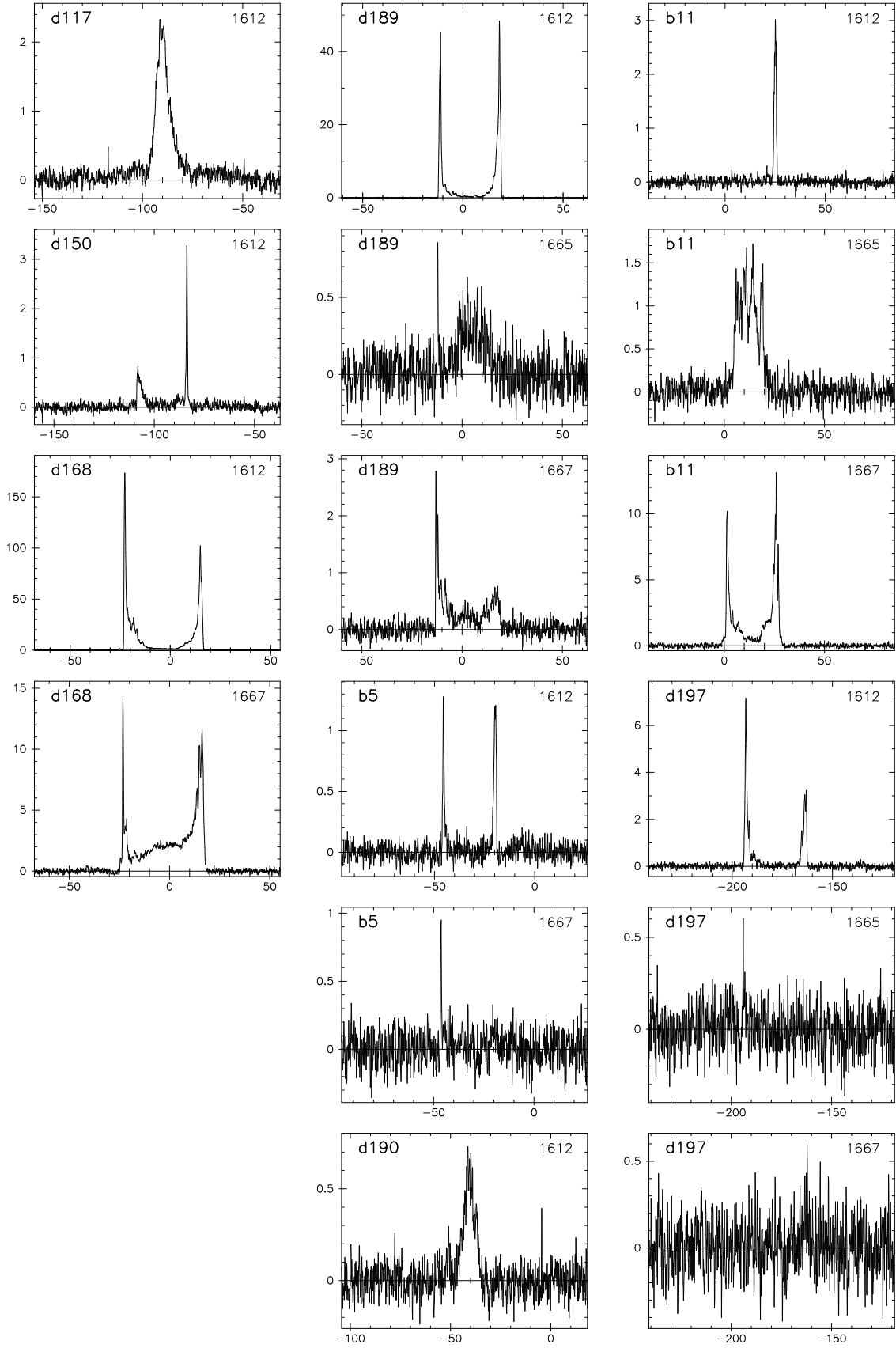


Fig. 6.— Examples of spectra from each classification category. The catalogue name of each star is given in the top right-hand corner with the category type given below the name.

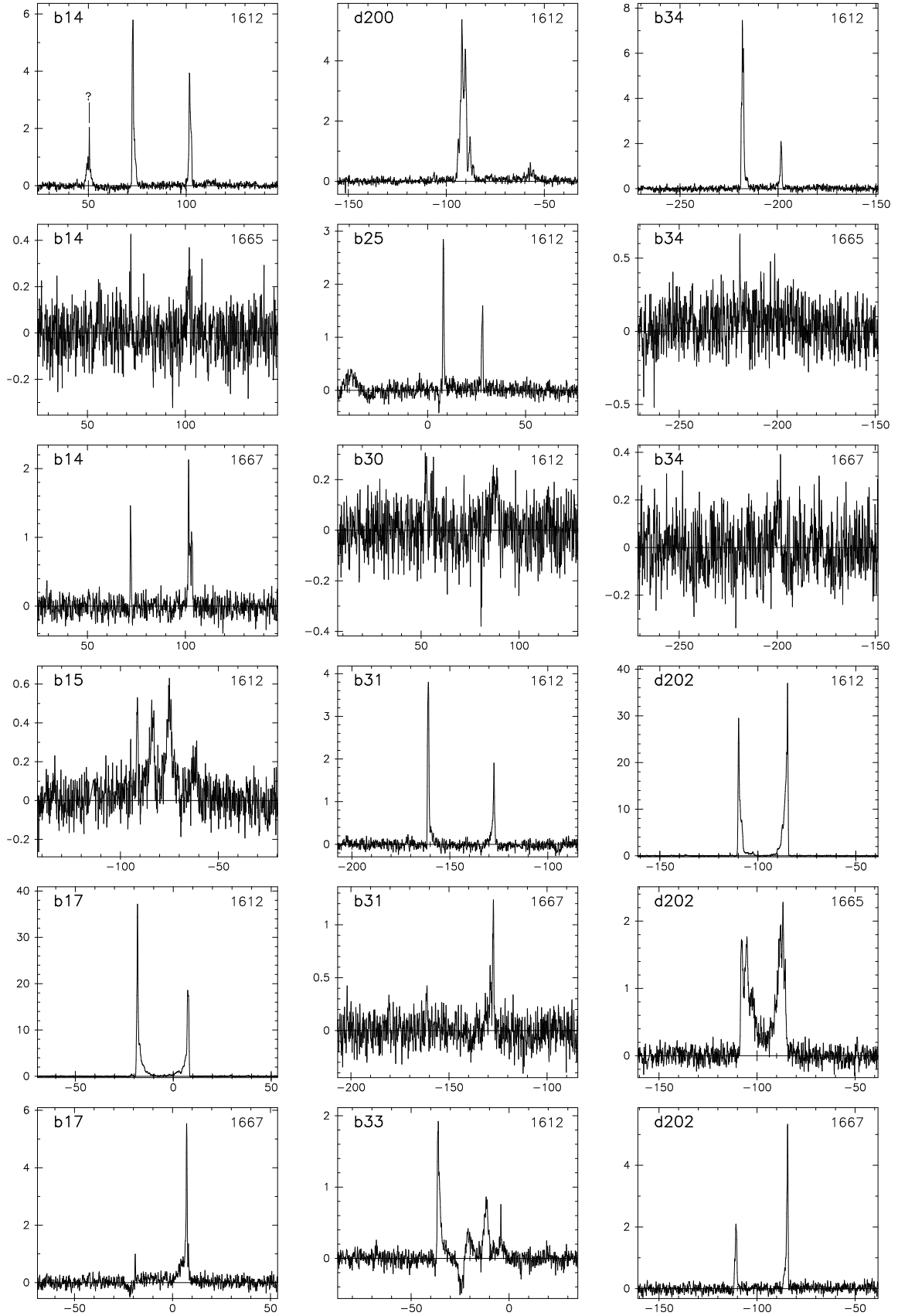
A. Appendix



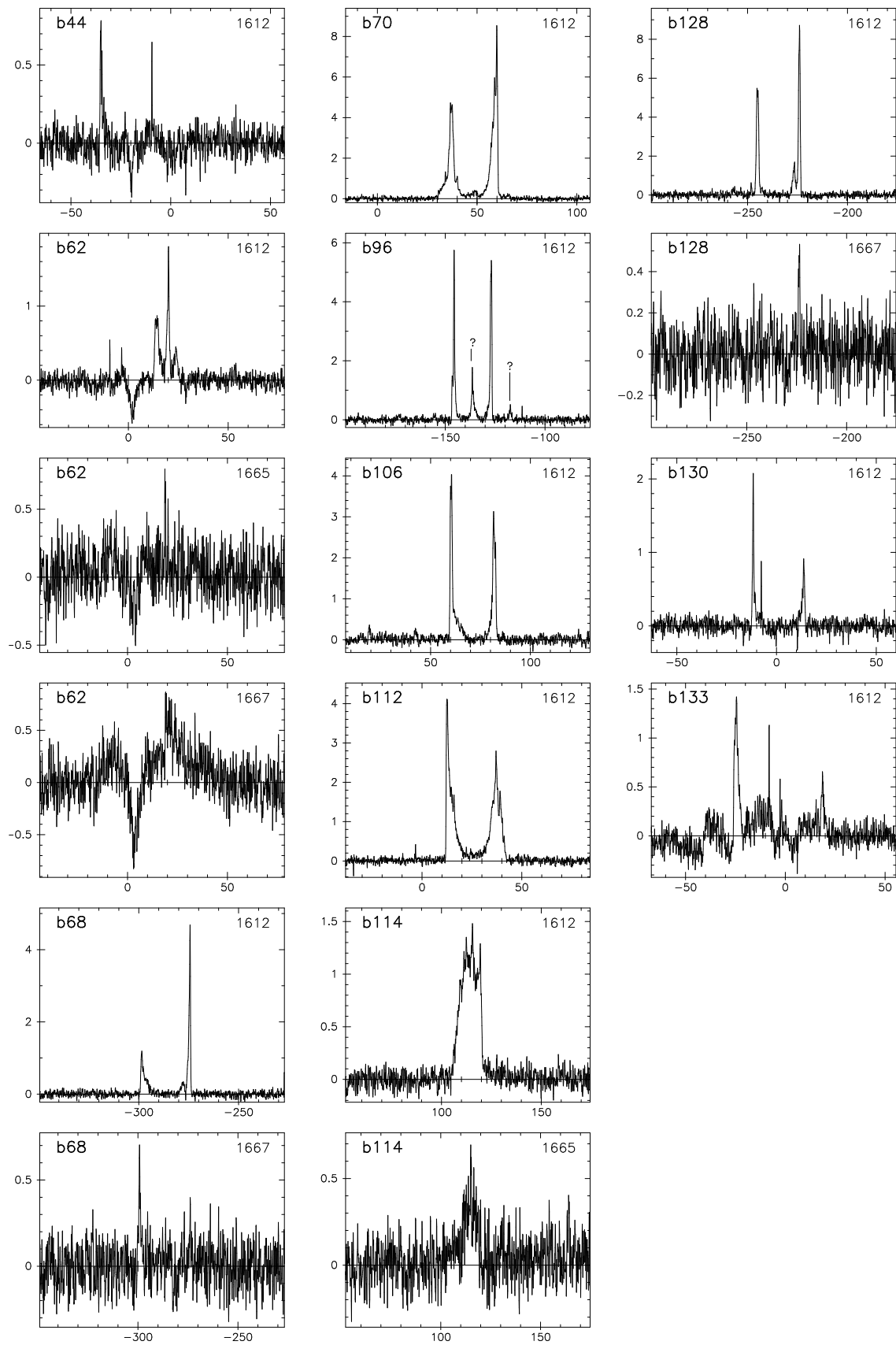
(a)



(b)



(c)



(d)

